Available online at www.sciencedirect.com
SCIENCE DIRECT®
Journal of Computational Physics 191 (2003) 341–376
JOURNAL OF COMPUTATIONAL PHYSICS
www.elsevier.com/locate/jcp

Semi-Lagrangian schemes for the Vlasov equation on an unstructured mesh of phase space

N. Besse [a,b,*], E. Sonnendrücker [b]

[a] Commissariat à l'Energie Atomique, DAM-Ile de France, BP No. 12, 91680 Bruyères-le-Châtel, France
[b] Institut de Recherche Mathematique Avancée, Université Louis Pasteur – CNRS, 7 rue René Descartes, 67084 Strasbourg Cedex, France

Received 9 October 2002; received in revised form 31 March 2003; accepted 9 June 2003

Abstract

A new scheme for solving the Vlasov equation using an unstructured mesh for the phase space is proposed. The algorithm is based on the semi-Lagrangian method which exploits the fact that the distribution function is constant along the characteristic curves. We use different local interpolation operators to reconstruct the distribution function f, some of which need the knowledge of the gradient of f. We can use limiter coefficients to maintain the positivity and the L^∞ bound of f and optimize these coefficients to ensure the conservation of the L^1 norm, that is to say the mass by solving a linear programming problem. Several numerical results are presented in two and three (axisymmetric case) dimensional phase space. The local interpolation technique is well suited for parallel computation.

Keywords: Vlasov–Poisson system; Semi-Lagrangian methods; Conservation laws; Plasma physics; Particle beams; Time splitting

1. Introduction

The Vlasov equation describes the evolution of a system of particles under the effects of self-consistent and applied electromagnetic fields. The unknown $f(t,x,v)$, where t stands for time, x for position and v for velocity, represents the distribution function of particles (ions, electrons, etc.) in phase space. The Vlasov equation is used to study collisionless plasma and the propagation of charged particle beams.

The numerical resolution of the Vlasov equation is most of the time performed by Lagrangian methods like particle in cell methods (PIC) which consist of approximating the plasma by a finite number of macro-particles. The trajectories of these particles are computed from characteristic curves given by the Vlasov equation, whereas self-consistent fields are computed by gathering the charge and

* Corresponding author.
E-mail addresses: nicolas.besse@cea.fr, besse@math.u-strasbg.fr (N. Besse), sonnen@math.u-strasbg.fr (E. Sonnendrücker).

0021-9991/$ - see front matter © 2003 Elsevier B.V. All rights reserved.
doi:10.1016/S0021-9991(03)00318-8

current densities of the the particles on a mesh of the physical space (see [6] for more details). Although this method allows to obtain satisfying results with a small number of particles, it is well known that the numerical noise inherent to the particle method becomes too significant to allow a precise description of the tail of the distribution function which plays an important role in charged particle beams. This numerical noise decreases in $1/\sqrt{N}$, when N, the number of particles increases. Note that the accuracy of PIC methods can be improved by averaging the results obtained from several runs with a reasonable computational cost. As another option, Eulerian methods, which consist in discretizing the Vlasov equation on a mesh of phase space have been proposed. For example a finite element method has been proposed in [33]. Although this method takes into account complicated boundaries, it is not a conservative method and it requires to solve a global linear system which makes it hard to use in high dimension as global resolution is too long. Another method called Fourier–Fourier transform, based on the Fourier transform of the distribution function in phase space, works for periodic boundaries condition, but for nonperiodic problems Gibbs oscillations become a source of spurious oscillations which propagate into the distribution function (see [21]). Other methods like the flux balance method (FBM) [15,26] are based on the computation of the average of the Vlasov equation on each cell of the grid by a conservative method like the finite volume method. The techniques used to reconstruct the distribution function do not preserve the positivity which is an inconvenience for large simulations. The Piecewise Parabolic Method (PPM) [12] and the Van-Leer-Limited scheme (VL) [1] use limiters (slope limiter for VL) on the geometrical reconstruction of the distribution function to maintain monotonicity and positivity whereas the flux corrected transport (FCT) [7] achieves this by flux limiter. The reconstruction is linear for VL and parabolic for PPM. A similar geometrical reconstruction of third order which leads to the positive flux conservative method (PFC) is used in [16] but the scheme imposes positivity and not monotonicity. These methods are first order and dissipative in areas where the limiter acts (near extrema) and formally high order elsewhere. A comparison of Eulerian-grid-based Vlasov solvers can be found in [1,17]. An other kind of Eulerian method is the semi-Lagrangian method (see [32]) consisting in computing directly the distribution function on a Cartesian grid of phase space. This computation is done by integrating the characteristic curves backward at each time step and interpolating the value at the feet of the characteristics by a cubic spline method or a Lagrange interpolation scheme. Nakamura and Yabe proposed the cubic interpolated propagation (CIP) [27] method based on the approximation of the gradients of the distribution function in order to use the one-dimensional Hermite interpolation. These methods are high order and preserve the global mass but they are not positive and monotone.

In this paper, we propose a new method based on the semi-Lagrangian principle for solving the Vlasov equation on an unstructured mesh in phase space. This method works with different kinds of high order local interpolation operators requiring the knowledge of the gradients which are obtained by advecting them. Moreover we use ideas developed in numerical weather prediction codes by Priestley [29] and Gravel and Staniforth [31] to get a positive and conservative method by introducing a local linear combination of low order solution and high order solution.

This paper is organized as follows. In the first part we recall the Vlasov equation and some properties of the solution. Then we present the numerical method based on semi-Lagrangian ideas. In Section 4, we present numerical results in two and three-dimensional phase space in the field of collisionless plasma and charged particle beams.

2. The Vlasov equation

The evolution of the distribution function of particles $f(t,x,v)$ in phase space $(x,v) \in \mathbb{R}^d \times \mathbb{R}^d$, $d = 1,\ldots,3$, is given by the Vlasov equation

$$\frac{\partial f}{\partial t} + v \cdot \nabla_x f + F(t,x,v) \cdot \nabla_v f = 0, \tag{1}$$

where the force field $F(t,x,v)$ is coupled with the distribution function f giving a nonlinear system. We recall two well-known models, Vlasov–Poisson (VP) and Vlasov–Maxwell (VM) which describes the evolution of charged particles under the effects of self-consistent electromagnetic fields.

The coupling between f and the force field is done by the source terms ρ, the charge density, and j, the current density which are given by

$$\rho(t,x) = q \int_{\mathbb{R}^d} f(t,x,v)\,\mathrm{d}v, \quad j(t,x) = q \int_{\mathbb{R}^d} v f(t,x,v)\,\mathrm{d}v.$$

For the (VP) system the force field is given by

$$F(t,x,v) = \frac{q}{m} E(t,x), \quad E(t,x) = -\nabla_x \phi(t,x), \quad -\varepsilon_0 \Delta \phi(t,x) = \rho(t,x),$$

where q and m are, respectively, the charge and the mass of one particle.

For the (VM) system the force field is the Lorentz force given by

$$F(t,x,v) = \frac{q}{m}(E(t,x) + v \wedge B(t,x)),$$

where E and B solve the Maxwell equations.

Now we recall the classical a priori estimates for the (VP) and (VM) system. If $f_0(x,v)$ is positive then $f(t,x,v)$ remains positive for all $t \geqslant 0$. By observing that $\mathrm{div}_v F(t,x,v) = 0$, if f is smooth enough, then for all function $\beta \in \mathscr{C}^1(\mathbb{R}^+, \mathbb{R}^+)$,

$$\int_{\mathbb{R}^d \times \mathbb{R}^d} \beta(f(t,x,v))\,\mathrm{d}x\,\mathrm{d}v$$

is constant for all $t \geqslant 0$. Especially, all L^p norms, $1 \leqslant p \leqslant \infty$, are preserved. Moreover if we take $\beta(r) = r \ln r$, we get the conservation of the kinetic entropy defined by

$$H(t) = \int_{\mathbb{R}^d \times \mathbb{R}^d} f(t,x,v) \ln f(t,x,v)\,\mathrm{d}x\,\mathrm{d}v \quad \forall t > 0.$$

Next, multiplying the Vlasov equation by $|v|^2$, and integrating by parts we find the conservation of energy which is given by

$$\frac{m}{2} \int_{\mathbb{R}^d \times \mathbb{R}^d} f(t,x,v)|v|^2\,\mathrm{d}x\,\mathrm{d}v + \frac{\varepsilon_0}{2} \int_{\mathbb{R}^d} |E(t,x)|^2\,\mathrm{d}x \quad \forall t > 0$$

for the (VP) system and

$$\frac{m}{2} \int_{\mathbb{R}^d \times \mathbb{R}^d} f(t,x,v)|v|^2\,\mathrm{d}x\,\mathrm{d}v + \varepsilon_0 \int_{\mathbb{R}^d} \frac{|E(t,x)|^2 + c^2|B(t,x)|^2}{2}\,\mathrm{d}x \quad \forall t > 0, \ \ \varepsilon_0 \mu_0 c^2 = 1$$

for the (VM) system. Finally the total mass and impulsion

$$\int_{\mathbb{R}^d \times \mathbb{R}^d} f(t,x,v) \begin{pmatrix} 1 \\ v \end{pmatrix} \mathrm{d}v\,\mathrm{d}x$$

are conserved.

If $a(t,x,v) = (v, F(t,x,v))^{\mathrm{T}}$ is sufficiently smooth (Lipschitz continuous), then we can define unique characteristic curves $(X(s,x,v;t), V(s,x,v;t))$ of the first-order differential operator,

$$\frac{\partial}{\partial t} + a \cdot \nabla,$$

which solve the following system of ordinary differential equations

$$\begin{cases} \dfrac{\mathrm{d}X}{\mathrm{d}t}(s,x,v;t) = V(s,x,v;t), \\ \dfrac{\mathrm{d}V}{\mathrm{d}t}(s,x,v;t) = F(t,X(s,x,v;t),V(s,x,v;t)), \\ X(s,x,v;s) = x, V(s,x,v;s) = v, \end{cases} \tag{2}$$

where $(X(s,x,v;t), V(s,x,v;t))$ denotes the position in phase space at the time t, of a particle which was at (x,v) at time s.

Since $\mathrm{div}_{(x,v)} a = 0$, we can rewrite the Vlasov equation in the conservative form

$$\frac{\partial f}{\partial t} + \mathrm{div}_{(x,v)}(af) = 0 \quad \forall (t,x,v) \in \mathbb{R}^+ \times \mathbb{R}^d \times \mathbb{R}^d \tag{3}$$

with the initial condition

$$f(0,x,v) = f_0(x,v). \tag{4}$$

In [8] it is proved that the Jacobian $J(s,x,v;t) = \det(\partial_{(x,v)}(X(s,x,v;t), V(s,x,v;t))$ remains positive, bounded and verifies the equation

$$\frac{\partial J}{\partial t} = J(\mathrm{div}_{(x,v)} a)(t, X(s,x,v;t), V(s,x,v;t)).$$

Then it is also proved that the solution of (3) is given by

$$f(t,x,v) = f(s, X(t,x,v;s), V(t,x,v;s)) J(t,x,v;s). \tag{5}$$

In the case of Vlasov equation, as $\mathrm{div}_{(x,v)} a = 0$, we get $J = 1$, and the flow $\varphi_t(x,v) = (X(s,.,.;t), V(s,.,.;t))$ preserves the measure of the volume of the phase space so that Eq. (5) becomes

$$f(t,x,v) = f(s, X(t,x,v;s), V(t,x,v;s)).$$

This last equation means that the distribution function f is constant along the characteristic curves and it will be the starting point for our numerical method. A good review on the Cauchy problem in kinetic theory can be found in [18]. Especially, it is proven that if f_0 is smooth and compactly supported the solution of the VP system still remains smooth and compactly supported for all the time.

3. The numerical scheme

In this section, we present our numerical scheme, which is not restricted by a CFL (Courant–Friedrichs–Levy) condition as it is usually the case for the most classical Eulerian algorithms such as finite difference or finite volume schemes. The VP and the VM models are mixing systems whose evolution can become tremendously complex. Indeed the function remains constant along the trajectories but the characteristic curves becomes more and more intricate. Then different regions of phase space, where f has different values

come close together and steep gradients appear. The filamentation development is a problem as we loose information when the size of the filaments becomes smaller than the size of the cells. An unstructured mesh can present some advantages. Indeed, an unstructured mesh allows us to consider complicated boundaries, which arise for example in simulations of the propagation of charged particles beams in an accelerator with complex geometry. Moreover as the mesh is unstructured there is no privileged direction which could introduce a slant in physical results. Of course in this paper we use the fractional step method which gives more importance to the directions parallel to the axis but characteristic curves could also be solved by using classical numerical methods for integrating an ordinary differential equation like Euler or Runge–Kutta schemes for example. In this case there is no more privileged direction. Since the integration is done backward this method leads to a fixed point problem for which convergence problems can arise. In some problems, physical phenomena stay contained in a certain volume of phase space whose boundaries can be more or less complex. Then an unstructured mesh of phase space allows to compute the solution only on the useful part of the phase space. For example, we know that a Kapchinsky–Vladirmisky (K–V) beam is contained in a hyper-ellipsoid. Moreover unstructured meshes like triangulations are very well suited for a priori local mesh refinement. Indeed, for some physical problems, during the whole time of the simulation we know the areas where the solution needs to be more precise. In order to get a better description of the physics, we can build a mesh with local refinement in these regions and put the computation effort only on judicious areas. For some rectangular grid schemes like PFC if we want to have a better resolution somewhere we need to add whole lines and therefore useless nodes.

The existence of the reversible Hamiltonian flow φ_t, solution of particles trajectories (2), implies the existence of an evolution operator $\mathscr{S}$ (which has the properties of a semi-group) acting on sufficiently smooth function such that

$$f(t,x,v) = \mathscr{S}(t)f_0(x,v) = f_0\big(\varphi_t^{-1}(x,v)\big), \quad \varphi_t \cdot \varphi_t^{-1} = \text{identity}. \tag{6}$$

Therefore, the discretization in time is based on the Strang splitting scheme which gives an approximation of order two in time of $\mathscr{S}$. It can be written as follows

$$\mathscr{S}(\Delta t) = \mathscr{S}_x(\Delta t/2)\bigcirc\mathscr{S}_v(\Delta t)\bigcirc\mathscr{S}_x(\Delta t/2) + \mathrm{O}(\Delta t^2),$$

where

$$\mathscr{S}_x(\Delta t)f(x,v) = f(x - v\Delta t, v) \quad \text{and} \quad \mathscr{S}_v(\Delta t)f(x,v) = f(x, v - F(x)\Delta t).$$

In other words, the Strang splitting scheme consists in solving successively a half advection in physical space, an advection in velocity space and another half advection in physical space. Depending on the interpolation operator we use, we advect not only the distribution function f but also the gradients of f because we need them to reconstruct f everywhere. The equations to update the gradients are obtained by differentiating the solution of the transport equation. In other words the gradients are solution of a transport problem too. Indeed the transport equations for the gradients are obtained by differentiating the Vlasov equation, where each equation is solved by a splitting method. The set of equations

$$\begin{cases} \partial_t(\nabla_x f) + (v\cdot\nabla_x)\nabla_x f + \nabla_x E\nabla_v f + (E\cdot\nabla_v)\nabla_x f = 0, \\ \partial_t(\nabla_v f) + \nabla_v v\nabla_x f + (v\cdot\nabla_x)\nabla_v f + (E\cdot\nabla_v)\nabla_v f = 0 \end{cases}$$

is replaced by

$$(P_x)\begin{cases} \partial_t(\nabla_v f) + (v\cdot\nabla_x)\nabla_v f = 0 & (P_x^1) \\ \partial_t(\nabla_x f) + (v\cdot\nabla_x)\nabla_x f = 0 & (P_x^2) \\ \partial_t(\nabla_v f) = -\nabla_v v\nabla_x f & (P_x^3) \end{cases}$$

and

$$(P_v)\begin{cases} \partial_t(\nabla_x f) + (E\cdot\nabla_v)\nabla_x f = 0 & (P_v^1)\\ \partial_t(\nabla_v f) + (E\cdot\nabla_v)\nabla_v f = 0 & (P_v^2)\\ \partial_t(\nabla_x f) = -\nabla_x E\nabla_v f & (P_v^3)\end{cases}.$$

First we solve the system P_x on a half time step, then we solve the system P_v on a time step, and finally we solve again the system P_x on a half time step. The advection equations, (P_x^1), (P_v^1), (P_x^2), (P_v^2), can be integrated exactly in time. For the equation (P_x^3), (P_v^3), we use and explicit Euler scheme in time. The initial condition for each system is given by the the solution of the previous system. Each advection is easy to perform since the characteristic curves can be solved exactly. The error of time discretization comes from the way we carry out the splitting (see [22]). A convergence proof of a such semi-Lagrangian method with gradient propagation for the nonlinear VP system can be found in [5]. First we describe the algorithm which gives the semi-discretization in time of the numerical scheme and allows to go from time step t^n to t^{n+1}.

1. Perform a half time step advection in physical space:

$$\begin{aligned} f^\star(x,v) &= f(t^n, x - v\Delta t/2, v),\\ \nabla_x f^\star(x,v) &= \nabla_x(f(t^n, x - v\Delta t/2, v))\\ &= \nabla_x f(t^n, x - v\Delta t/2, v),\\ \nabla_v f^\star(x,v) &= \nabla_v(f(t^n, x - v\Delta t/2, v))\\ &= -\frac{\Delta t}{2}\nabla_x f(t^n, x - v\Delta t/2, v) + \nabla_v f(t^n, x - v\Delta t/2, v). \end{aligned}$$

2. Compute the electric field $E^\star(x)$ by substituting $f^\star$ in the Poisson equation; that is to say, solve the following system:

$$\begin{cases} E^\star(x) = -\nabla_x\phi^\star(x),\\ -\Delta\phi^\star(x) = \rho^\star(x),\\ \rho^\star(x) = \int_{\mathbb{R}^d} f^\star(x,v)\,\mathrm{d}v. \end{cases}$$

3. Perform a full time step advection in velocity space:

$$\begin{aligned} f^{\star\star}(x,v) &= f^\star(x, v - E^\star(x)\Delta t),\\ \nabla_x f^{\star\star}(x,v) &= \nabla_x(f^\star(x, v - E^\star(x)\Delta t))\\ &= \nabla_x f^\star(x, v - E^\star(x)\Delta t) - \Delta t\nabla E^\star(x)\nabla_v f^\star(x, v - E^\star(x)\Delta t),\\ \nabla_v f^{\star\star}(x,v) &= \nabla_v(f^\star(x, v - E^\star(x)\Delta t))\\ &= \nabla_v f^\star(x, v - E^\star(x)\Delta t). \end{aligned}$$

4. Perform a second half time step advection in physical space:

$$\begin{aligned} f(t^{n+1}, x, v) &= f^{\star\star}(x - v\Delta t/2, v),\\ \nabla_x f(t^{n+1}, x, v) &= \nabla_x(f^{\star\star}(x - v\Delta t/2, v))\\ &= \nabla_x f^{\star\star}(x - v\Delta t/2, v),\\ \nabla_v f(t^{n+1}, x, v) &= \nabla_v(f^{\star\star}(x - v\Delta t/2, v))\\ &= -\frac{\Delta t}{2}\nabla_x f^{\star\star}(x - v\Delta t/2, v) + \nabla_v f^{\star\star}(x - v\Delta t/2, v). \end{aligned}$$

At each advection step, once we have followed the characteristic curves backward we have to evaluate the distribution function f and its gradients at the end points of the characteristic curves which are generally not the nodes of the mesh where we know f. Therefore we have to reconstruct f by an interpolation technique. Next, we present different local interpolation operators which are used to reconstruct f. Some of them need only the knowledge of f at the mesh nodes like Lagrange interpolation but for others we need to know not only f but also ∇f at the mesh points.

Note that in step 3 of the algorithm we have to know the gradient of the electric field which is a 2×2 matrix in two dimensions and a 3×3 matrix in three dimensions. In the numerical cases we consider, we do not need to compute directly the gradient of the electric field or the gradient of the force applied to the particles because we can deduce it from other physical quantities. Nevertheless, in the general case we have to compute the gradient of the force applied to the particles. In the context of the coupling with the Poisson equation, as the force applied to the particles is the electric force, and since the Poisson problem is linear we obtain the gradient of the electric field by differentiating the Poisson system,

$$\begin{cases} \nabla_x E^\star(x) = -\nabla_x\big(\nabla_x \phi^\star(x)\big), \\ -\Delta\big(\nabla_x \phi^\star(x)\big) = \nabla_x \rho^\star(x), \\ \nabla_x \rho^\star(x) = \int_{\mathbb{R}^d} \nabla_x f^\star(x,v)\,\mathrm{d}v, \end{cases}$$

which for example can be solved by a finite element method.

Let Ω be the compact domain of $\mathbb{R}_x \times \mathbb{R}_v$, where we want to compute the solution, and $\mathscr{T}_h$ be a triangulation of Ω. An element T, of the triangulation is a triangle of $\mathbb{R}^2$ defined by its three vertex $\{a_i\}_{i=1,\ldots,3}$. Every point P of $\mathbb{R}^2$ is characterized by its Cartesian coordinates (x,v) and its barycentric coordinates $\lambda_j = \lambda_j(x,v)$, $1 \leqslant j \leqslant 3$, which are linked by the equation

$$\forall (x,v) \in \mathbb{R}^2 \quad (x,v) = \sum_{j=1}^{3} \lambda_j(x,v) a_j.$$

We first present Lagrange interpolation, which does not need to propagate the gradients. Nevertheless we will see later that this kind of reconstruction leads to stability problems. Therefore we present local interpolation techniques which involve the propagation of f and ∇f, and give more stable reconstruction. Most of these interpolation techniques come from the finite element literature [2,11,28].

3.1. Lagrange interpolation

In order to define the Lagrange interpolation of order k on a triangle T, we need to define the principal lattice of order k which is the set of the points of $\mathbb{R}^2$ determined by

$$L_k(T) = \left\{ (x,v) \in \mathbb{R}^2;\ \lambda_j(x,v) \in \left\{ 0, \frac{1}{k}, \ldots, \frac{k-1}{k}, 1 \right\},\ 1 \leqslant j \leqslant 3 \right\},$$

where the barycentric coordinates are defined with respect to the vertex $\{a_i\}_{i=1,\ldots,3}$. Every point of the principal lattice $L_k(T)$ can be written as

$$a_\mu = \frac{1}{k} \sum_{j=1}^{3} \mu_j a_j, \quad \mu = (\mu_1, \mu_2, \mu_3),$$

where the coefficients μ_j are integer which verify the relations

$$\mu_j \geqslant 0, \quad \sum_{j=1}^{3} \mu_j = k.$$

We associate $L_k(T)$ with the set of degrees of freedom $\Sigma_k(T)$ defined as follows

$$\Sigma_k(T) = \{f(a_\mu),\ a_\mu \in L_k(T)\}$$

and with the space of Lagrange polynomial of order k, $P_k(T)$ whose dimension is $(2+k)!/2!k!$ which is identical to the cardinal of $L_k(T)$. $P_k(T)$ is defined by its basis functions φ_μ as follows. We associate every vertex a_μ of $L_k(T)$ with the basis function φ_μ defined by

$$\varphi_\mu(x,v) = \left(\prod_{j=1}^{3}(\mu_j!)\right)^{-1} \prod_{\substack{j=1 \\ \mu_j \geqslant 1}}^{3} \prod_{i=0}^{\mu_j-1}(k\lambda_j(x,v) - i). \tag{7}$$

The triple $(T, P_k(T), \Sigma_k(T))$ is called a Lagrange finite element. Then we introduce the local interpolation operator Π_T defined by

$$(\Pi_T f)(x,v) = \sum_{\mu=1}^{N_k} f(a_\mu)\varphi_\mu(x,v) \quad \forall f \in \mathscr{C}^0(\overline{T}) \tag{8}$$

with $N_k = (2+k)!/2!k!$ and φ_μ is defined by (7). Now we introduce the space X_h, which will be the space of the discretization of the solution:

$$X_h = \left\{ f \in \mathscr{C}^0(\overline{\Omega}) \cap H^1(\Omega);\ f_{|_{T_j}} \in P_k(T_j)\ \forall T_j \in \mathscr{T}_h \right\}.$$

The space X_h is characterized by the basis functions $\{\psi_k\}$, which verify the property $\psi_k(x_i, v_i) = \delta_{i,k}$, where (x_i, v_i) is the ith point of the triangulation $\mathscr{T}_h$. Then, every function $f \in X_h$ is given by

$$f(x,v) = \sum_k f(x_k, v_k)\psi_k(x,v).$$

Finally we define the global interpolation operator Π_h by

$$(\Pi_h f)(x,v) = \sum_{k=1}^{N} f_k \psi_k(x,v) \quad \forall f \in \mathscr{C}^0(\overline{\Omega}),$$

where $f_k = f(x_k, v_k)$ and N is the number of all degrees of freedom.

The relationship of paramount importance between the global interpolation operator Π_h and the local interpolation operator Π_T is given by

$$(\Pi_h v)_{|_T} = \Pi_T\left(v_{|_T}\right)\ \forall T \in \mathscr{T}_h,\ \ v \in \mathscr{C}^0(\overline{\Omega}), \tag{9}$$

where $v_{|_T}$ denotes the restriction of v onto T.

In fact Lagrange interpolation of high order on triangles does not provide a good reconstruction for the distribution function since the Lagrange interpolation operator does not have good stability properties. If we take a one-dimensional finite element (a bounded interval) it is well known that the Lagrange interpolant oscillates a lot at the extremities of the element, even if the function to interpolate is very smooth. Besides the amplitude of the oscillations increase with the degree of the Lagrange polynomial. This observation is known as the Runge phenomena. For example Runge has consider the Cauchy distribution

$$f(x) = \frac{1}{1+x^2}$$

in the interval [−5,5], with the equally spaced points

$$x_j = -5 + j\Delta x, \quad j = 0, 1, 2, \ldots, n, \ \ \Delta x = \frac{10}{n}.$$

For each n there exists a unique polynomial $P_n(x)$ of degree at most n such that $P_n(x_j) = f(x_j)$. This is the Lagrange interpolation polynomial. In [20] it is shown that $|f(x) - P_n(x)|$ becomes arbitrarily large at points in [−5,5] if n is sufficiently large. Moreover this occurs even though the interpolation points $\{x_j\}$ become dense in [−5,5] as $n \to \infty$. Then it means that the ratio of $\|P_n\|_{L^\infty}$ to $\|f\|_{L^\infty}$ is greater than one and increases with n. If $\{\ell_i\}_{i=0,n}$ denote the Lagrange basis functions and π_h the Lagrange interpolation operator in one dimension, we have

$$\|\pi_h\|_{L^\infty} = \sup_{\substack{f \in \mathscr{C}([a,b]) \\ f \neq 0}} \frac{\|P_n\|_{L^\infty}}{\|f\|_{L^\infty}} = \sup_{x \in [a,b]} \sum_{i=0}^{n} |l_i(x)| = C > 1,$$

where C is independent of the discretization parameter h, but dependent on n, the order of the Lagrange polynomials. If we take a uniform discretization we can prove that (see [13,24])

$$\|\pi_h\|_{L^\infty} \sim 1 + \frac{2^{n+1}}{en\log n},$$

which can be optimized when the interpolation points are the zeros of Chebyshev polynomials of degree $n+1$, then the stability constant becomes

$$\|\pi_h\|_{L^\infty} \sim 1 + \frac{2}{\pi}\log n.$$

Therefore it is impossible to get stability in the sense there is constant C such that

$$\|\Pi_h g\|_{L^\infty(\Omega)} \leqslant (1 + Ch)\|g\|_{L^\infty(\Omega)} \quad \forall g \in L^\infty(\Omega), \tag{10}$$

where h is the maximum diameter of the triangles and Π_h a high order Lagrange interpolation operator (order >1). Moreover the same estimates as (10) seems difficult to obtain in other Lebesgue L^p space with $p \in [1, \infty]$. The stability condition (10) is a crucial estimate to obtain convergence of the numerical method (see [3]). Nevertheless we can show (see [4]) that the stability condition (10) holds when we replace the L^∞ norm by the L^2 norm, with symmetrical Lagrange interpolation of any order on a grid. More precisely, it is shown that L^2-stability only holds if the feet of the characteristics fall in a certain area centered in the finite element. Then if we symmetrize Lagrange interpolation we can recover L^2-stability. Even if the same kind of result probably exists on unstructured meshes (triangulation) it is useless in practice as we cannot control where the foot of a characteristic falls in a triangle. The proof of such a result is very complex as there are no convenient tools to study the L^2-stability on unstructured meshes. We now consider Hermite type interpolation which are not subject to this problem.

3.2. Hermite type interpolation

In order to use local interpolation operators we have to define the triple (T, P_T, Σ_T). Depending on which interpolation operator is considered the space of discretization of the solution will be, respectively

$$X_h = \left\{ f \in \mathscr{C}^0(\overline{\Omega}) \cap H^1(\Omega);\ f_{|_{T_j}} \in P_T(T_j)\ \forall T_j \in \mathscr{T}_h \right\}$$

or

$$Y_h = \left\{ f \in \mathscr{C}^1(\overline{\Omega}) \cap H^2(\Omega); f_{|_{T_j}} \in P_T(T_j)\ \forall T_j \in \mathscr{T}_h \right\}.$$

Then we present different local interpolation operators which require the knowledge of f and ∇f. In fact we just have to define Σ_T and Π_T. Next we denote, respectively, by P_2 and P_3 the sets of polynomials of degree two and three. Finally we introduce the notation mod where $i \bmod j = i - \mathrm{int}(i/j) * j$. The solution of the continuous problem is supposed to be smooth, typically in $\mathscr{C}^m(\overline{\Omega})$. In velocity space the solution is rapidly decreasing and in physical space the solution is periodic or rapidly decreasing. Note that all these properties have to be verified by the initial data so as to hold for all finite times.

3.2.1. The $\mathscr{C}^0$ reduced Hermite element (HC0)

The set of degrees of freedom is given by

$$\Sigma_T = \{ f(a_i) : 1 \leqslant i \leqslant 3; \partial_x f(a_i), \partial_v f(a_i) : 1 \leqslant i \leqslant 3 \},$$

and the local interpolation operator Π_T is determined for all f in $\mathscr{C}^0(\overline{T})$ by

$$\begin{aligned}\Pi_T f = \sum_{i=1}^{3} f(a_i)\big(-2\lambda_i^3 + 3\lambda_i^2 + 2\lambda_i\lambda_j\lambda_k \big) + \frac{\lambda_i\lambda_j}{2}(\lambda_i - \lambda_j + 1)\nabla f(a_i)\cdot(a_j - a_i) \\ + \frac{\lambda_i\lambda_k}{2}(\lambda_i - \lambda_k + 1)\nabla f(a_i)\cdot(a_k - a_i),\end{aligned}$$

where $\{\lambda_i\}_{i=1,\ldots,3}$ are the barycentric coordinates, $j = i \bmod 3 + 1$, and $k = j \bmod 3 + 1$. Note that $P_2 \subset P_T \subset P_3$. In fact $\Pi_T f$ is $\mathscr{C}^1$ over $\overline{T}$ except through the edges (see [11]).

3.2.2. The $\mathscr{C}^0$ cubic Nielson element (NC0)

The set of degrees of freedom is given by

$$\Sigma_T = \{ f(a_i) : 1 \leqslant i \leqslant 3; \partial_x f(a_i), \partial_v f(a_i) : 1 \leqslant i \leqslant 3 \},$$

and the local interpolation operator Π_T is determined for all f in $\mathscr{C}^0(\overline{T})$ by

$$\begin{aligned}\Pi_T f = \sum_{i=1}^{3} f(a_i)\big(-2\lambda_i^3 + 3\lambda_i^2 + 2\lambda_i\lambda_j\lambda_k \big) + \lambda_i\lambda_j\left(\lambda_i + \frac{1}{2}\lambda_k\right)\nabla f(a_i)\cdot(a_j - a_i) \\ + \lambda_i\lambda_k\left(\lambda_i + \frac{1}{2}\lambda_j\right)\nabla f(a_i)\cdot(a_k - a_i),\end{aligned}$$

where $j = i \bmod 3 + 1$, $k = j \bmod 3 + 1$, and $P_2 \subset P_T \subset P_3$. In fact $\Pi_T f$ is $\mathscr{C}^1$ over $\overline{T}$ except through the edges (see [28]).

3.2.3. The $\mathscr{C}^1$ cubic Nielson rational singular element (NC1)

The set of the degrees of freedom is given by

$$\Sigma_T = \{ f(a_i) : 1 \leqslant i \leqslant 3; \partial_x f(a_i), \partial_v f(a_i) : 1 \leqslant i \leqslant 3 \},$$

and the local interpolation operator Π_T is determined for all f in $\mathscr{C}^1(\overline{T})$ by

$$\begin{aligned}\Pi_T f = \sum_{i=1}^{3} f(a_i)(\lambda_i^2(3 - 2\lambda_i) + 6w\lambda_i(\lambda_k\alpha_{ij} + \lambda_j\alpha_{ik})) + \nabla f(a_i)\cdot(a_j - a_i)\left[\lambda_i^2\lambda_j + w\lambda_i(3\lambda_j\alpha_{ik} + \lambda_k - \lambda_j)\right] \\ + \nabla f(a_i)\cdot(a_k - a_i)\left[\lambda_i^2\lambda_k + w\lambda_i(3\lambda_k\alpha_{ij} + \lambda_j - \lambda_k)\right],\end{aligned}$$

where

$$w = \frac{\lambda_1\lambda_2\lambda_3}{\lambda_1\lambda_2 + \lambda_2\lambda_3 + \lambda_1\lambda_3},$$

$$\alpha_{ij} = \frac{||e_i||^2 + ||e_j||^2 - ||e_k||^2}{2||e_j||^2},$$

and $||e_i||$ denote the length of edge e_i opposite to the vertex a_i. We have the relationship $P_2 \subset P_T \subset P_3$. In fact we recover the $\mathscr{C}^1$ continuity through the edge by adding rational polynomials (see [11,28]). Moreover NC1 operator has a good stability property since it is a discretization of the operator $\mathscr{M}[f]$ characterized as the unique interpolant which minimizes the pseudonorm

$$\left(\int_T \left| \frac{\partial^2 f}{\partial x \partial v}(x,v) \right|^2 \mathrm{d}x\,\mathrm{d}v \right)^{1/2}$$

among all functions in $\mathscr{C}^4(T)$ which interpolate to $f \in \mathscr{C}^4(T)$ and its first derivative on the boundary of T (see [28]).

3.2.4. The $\mathscr{C}^1$ cubic Hsieh–Clough–Tocher element (HCT-C)

If a_i is a vertex of a triangle T, then we denote, respectively, by l_i, and m_i the length and the middle of the edge of T opposite to the vertex a_i. We denote by h_i the intersection point of the edge opposite to the vertex a_i and the perpendicular to this edge which goes through a_i. Then we introduce $n_i = |h_i - a_i|$ and v_i the unit exterior normal of the edge opposite to a_i. Let a be the barycentre of T, then K_i denotes the subtriangle of T built with the vertex a, a_j, and a_k where $1 \leqslant i \leqslant 3$, $j = i \bmod 3 + 1$ and $k = j \bmod 3 + 1$. Finally we introduce the so-called "eccentricity parameters" e_i defined by

$$e_i = \frac{l_k^2 - l_j^2}{l_i^2}.$$

The set of the degrees of freedom is given by

$$\Sigma_T = \{f(a_i) : 1 \leqslant i \leqslant 3; \partial_x f(a_i), \partial_v f(a_i), \partial_{v_i} f(m_i) : 1 \leqslant i \leqslant 3\},$$

where ∂_{v_i} denote the normal derivative. We can replace Σ_T by Σ_T' where

$$\Sigma_T' = \{f(a_i) : 1 \leqslant i \leqslant 3; \partial_x f(a_i), \partial_v f(a_i), \partial_x f(m_i), \partial_v f(m_i) : 1 \leqslant i \leqslant 3\}.$$

The local interpolation operator Π_T is determined for all f in $\mathscr{C}^1(\overline{T})$ by

$$\Pi_T f_{|K_l} = \sum_{i=l}^{(l+1) \bmod 3+1} f(a_i)\Psi_{l,i}^0 + \left(\nabla f(a_i) \cdot \overrightarrow{a_i a_k}\right)\Psi_{l,i,k}^1 + \left(\nabla f(a_i) \cdot \overrightarrow{a_i a_j}\right)\Psi_{l,i,j}^1 + \left(\nabla f(m_i) \cdot \overrightarrow{h_i a_i}\right)\Psi_{\perp,l,i}^1$$

or by

$$\Pi_T f_{|K_l} = \sum_{i=l}^{(l+1) \bmod 3+1} f(a_i)\Psi_{l,i}^0 + \left(\nabla f(a_i) \cdot \overrightarrow{a_i a_k}\right)\Psi_{l,i,k}^1 + \left(\nabla f(a_i) \cdot \overrightarrow{a_i a_j}\right)\Psi_{l,i,j}^1 - \left(n_i \frac{\partial f}{\partial v_i}(m_i)\right)\Psi_{\perp,l,i}^1.$$

The basis functions $\{\Psi_l\}$ are defined by

$$\Xi_l = \Sigma_l \Lambda_l$$

with $i = l$, $j = i \bmod 3 + 1$ and $k = j \bmod 3 + 1$

$$\Xi_l = (\Psi^0_{l,i}, \Psi^0_{l,j}, \Psi^0_{l,k}, \Psi^1_{l,i,k}, \Psi^1_{l,i,j}, \Psi^1_{l,j,i}, \Psi^1_{l,i,k}\Psi^1_{l,k,j}, \Psi^1_{l,k,i}, \Psi^1_{\perp,l,i}, \Psi^1_{\perp,l,j}, \Psi^1_{\perp,l,k})^{\mathrm{T}},$$

$$\Lambda_l = (\lambda_i^3, \lambda_j^3, \lambda_k^3, \lambda_i^2\lambda_k, \lambda_i^2\lambda_j, \lambda_j^2\lambda_i, \lambda_j^2\lambda_k, \lambda_k^2\lambda_j, \lambda_k^2\lambda_i, \lambda_i\lambda_j\lambda_k)^{\mathrm{T}}$$

and

$$\Sigma_l = \begin{bmatrix}
-\frac{1}{2}(e_j - e_k) & 0 & 0 & \frac{3}{2}(3 + e_j) & \frac{3}{2}(3 - e_k) & 0 & 0 & 0 & 0 & 0 \\
\frac{1}{2}(1 - 2e_i - e_k) & 1 & 0 & -\frac{3}{2}(1 - e_i) & \frac{3}{2}(e_i + e_k) & 3 & 3 & 0 & 0 & 3(3 - e_i) \\
\frac{1}{2}(1 + 2e_i - e_j) & 0 & 1 & -\frac{3}{2}(e_i + e_j) & -\frac{3}{2}(1 + e_i) & 0 & 0 & 3 & 3 & 3(3 + e_i) \\
-\frac{1}{12}(1 + e_j) & 0 & 0 & \frac{1}{4}(7 + e_j) & -\frac{1}{2} & 0 & 0 & 0 & 0 & 0 \\
-\frac{1}{12}(1 - e_k) & 0 & 0 & -\frac{1}{2} & \frac{1}{4}(7 - e_k) & 0 & 0 & 0 & 0 & 0 \\
-\frac{1}{12}(7 + e_k) & 0 & 0 & \frac{1}{2} & \frac{1}{4}(5 + e_k) & 1 & 0 & 0 & 0 & -1 \\
\frac{1}{6}(4 - e_i) & 0 & 0 & -\frac{1}{4}(3 - e_i) & -\frac{1}{4}(5 - e_i) & 0 & 1 & 0 & 0 & \frac{1}{2}(3 - e_i) \\
\frac{1}{6}(4 + e_i) & 0 & 0 & -\frac{1}{4}(5 + e_i) & -\frac{1}{4}(3 + e_i) & 0 & 0 & 1 & 0 & \frac{1}{2}(3 + e_i) \\
-\frac{1}{12}(7 - e_j) & 0 & 0 & \frac{1}{4}(5 - e_j) & -\frac{1}{2} & 0 & 0 & 0 & 1 & -1 \\
\frac{4}{3} & 0 & 0 & -2 & -2 & 0 & 0 & 0 & 0 & 4 \\
-\frac{2}{3} & 0 & 0 & 2 & 0 & 0 & 0 & 0 & 0 & 0 \\
-\frac{2}{3} & 0 & 0 & 0 & 2 & 0 & 0 & 0 & 0 & 0
\end{bmatrix}.$$

We have the equality $P_T = P_3$. For the proof of $\mathscr{C}^1$ continuity and the interpolation error estimates we refer to [11].

3.2.5. The $\mathscr{C}^1$ reduced cubic Hsieh–Clough–Tocher element (HCT-R)

With the same notations as previously the set of degrees of freedom is given by

$$\Sigma_T = \{f(a_i) : 1 \leqslant i \leqslant 3; \partial_x f(a_i), \partial_v f(a_i) : \ 1 \leqslant i \leqslant 3\}.$$

The local interpolation operator Π_T is determined for all f in $\mathscr{C}^1(\overline{T})$ by

$$\Pi_T f|_{K_l} = \sum_{i=l}^{(l+1) \bmod 3+1} f(a_i)\Psi^0_{l,i} + (\nabla f(a_i).\overrightarrow{a_i a_k})\Psi^1_{l,i,k} + (\nabla f(a_i).\overrightarrow{a_i a_j})\Psi^1_{l,i,j}.$$

The basis functions $\{\Psi_l\}$ are defined by

$$\Xi_l = \Sigma_l \Lambda_l$$

with $i = l$, $j = i \bmod 3 + 1$ and $k = j \bmod 3 + 1$

$$\Xi_l = (\Psi^0_{l,i}, \Psi^0_{l,j}, \Psi^0_{l,k}, \Psi^1_{l,i,k}, \Psi^1_{l,i,j}, \Psi^1_{l,j,i}, \Psi^1_{l,i,k}\Psi^1_{l,k,j}, \Psi^1_{l,k,i})^{\mathrm{T}},$$

$$\Lambda_l = (\lambda_i^3, \lambda_j^3, \lambda_k^3, \lambda_i^2\lambda_k, \lambda_i^2\lambda_j, \lambda_j^2\lambda_i, \lambda_j^2\lambda_k, \lambda_k^2\lambda_j, \lambda_k^2\lambda_i, \lambda_i\lambda_j\lambda_k)^{\mathrm{T}}$$

and

$$\Sigma_l = \begin{bmatrix} -\frac{1}{2}(e_j - e_k) & 0 & 0 & \frac{3}{2}(3+e_j) & \frac{3}{2}(3-e_k) & 0 & 0 & 0 & 0 & 0 \\ \frac{1}{2}(1-2e_i-e_k) & 1 & 0 & -\frac{3}{2}(1-e_i) & \frac{3}{2}(e_i+e_k) & 3 & 3 & 0 & 0 & 3(1-e_i) \\ \frac{1}{2}(1+2e_i-e_j) & 0 & 1 & -\frac{3}{2}(e_i+e_j) & -\frac{3}{2}(1+e_i) & 0 & 0 & 3 & 3 & 3(1+e_i) \\ -\frac{1}{4}(1+e_j) & 0 & 0 & \frac{1}{4}(5+e_j) & \frac{1}{2} & 0 & 0 & 0 & 0 & 0 \\ -\frac{1}{4}(1-e_k) & 0 & 0 & \frac{1}{2} & \frac{1}{4}(5-3e_k) & 0 & 0 & 0 & 0 & 0 \\ \frac{1}{4}(1-e_k) & 0 & 0 & -\frac{1}{2} & -\frac{1}{4}(1-3e_k) & 1 & 0 & 0 & 0 & 1 \\ -\frac{1}{2}e_i & 0 & 0 & -\frac{1}{4}(1-3e_i) & \frac{1}{4}(1+3e_i) & 0 & 1 & 0 & 0 & \frac{1}{2}(1-3e_i) \\ \frac{1}{2}e_i & 0 & 0 & \frac{1}{4}(1-3e_i) & -\frac{1}{4}(1+3e_i) & 0 & 0 & 1 & 0 & \frac{1}{2}(1+3e_i) \\ \frac{1}{4}(1+e_j) & 0 & 0 & -\frac{1}{4}(1+3e_j) & -\frac{1}{2} & 0 & 0 & 0 & 1 & 1 \end{bmatrix}.$$

We have the relationship $P_2 \subset P_T \subset P_3$. In fact HCT-R is obtained from HCT-C by supposing that the gradients vary linearly along the edges. For the proof of $\mathscr{C}^1$ continuity and the interpolation error estimates we refer to [11].

For smooth solution (with low gradients) like linear Landau damping the $\mathscr{C}^0$ and $\mathscr{C}^1$ reconstruction gives similar results. On the contrary for stiff problems (with steep gradients) like the two stream instability the $\mathscr{C}^0$ reconstructions does not give satisfactory results whereas the $\mathscr{C}^1$ reconstructions work well.

3.3. The fully discretized scheme

Now, we can write the fully discretized scheme. From the local interpolation operator Π_T we can define the global interpolation operator Π_h from $\mathscr{C}^0(\overline{\Omega})$ (resp. $\mathscr{C}^1(\overline{\Omega})$) onto X_h (resp. Y_h) by the relation (9). For example the discretization space Y_h built on the $\mathscr{C}^1$ cubic Nielson element admits basis functions $\{\varphi_k\}_{k=1,\dots,N}$, $\{\psi_k\}_{k=1,\dots,N}$ and $\{\eta_k\}_{k=1,\dots,N}$ such that

$$(\Pi_h f)(x,v) = \sum_{k=1}^{N} f_k \eta_k(x,v) + \partial_x f_k \psi_k(x,v) + \partial_v f_k \varphi_k(x,v) \quad \forall f \in \mathscr{C}^1(\overline{\Omega}),$$

where

$$f_k = f(x_k, v_k), \quad \partial_x f_k = (\partial_x f)(x_k, v_k), \quad \partial_v f_k = (\partial_v f)(x_k, v_k).$$

We start at the time t^n, where we know the discrete distribution function $f_h^n(x,v)$ that we can express as

$$f_h^n(x,v) = \sum_{k=1}^{N} f_{h,k}^n \eta_k(x,v) + \partial_x f_{h,k}^n \psi_k(x,v) + \partial_v f_{h,k}^n \varphi_k(x,v),$$

where the $\{f_{h,k}^n\}_{k=1}^N$, $\{\partial_x f_{h,k}^n\}_{k=1}^N$ and $\{\partial_v f_{h,k}^n\}_{k=1}^N$ are the degrees of freedom of the space Y_h. Now we develop the algorithm to reach time t^{n+1}.

1. Perform a half time step advection in physical space:

   $$f_h^\star(x,v) = \Pi_h f_h^n(x - v\Delta t/2, v),$$

   that is to say

   $$f_h^\star(x,v) = \sum_{k=1}^{N} f_{h,k}^\star \eta_k(x,v) + \partial_x f_{h,k}^\star \psi_k(x,v) + \partial_v f_{h,k}^\star \varphi_k(x,v),$$

   where

   $$f_{h,k}^\star = f_h^n(x_k - v_k \Delta t/2, v_k),$$

$$\partial_x f_{h,k}^{\star} = \partial_x f_h^n(x_k - v_k\Delta t/2, v_k),$$

$$\partial_v f_{h,k}^{\star} = -\frac{\Delta t}{2}\partial_x f_h^n(x_k - v_k\Delta t/2, v_k) + \partial_v f_h^n(x_k - v_k\Delta t/2, v_k).$$

2. Compute the electric field $E_h^{\star}(x)$ by substituting $f_h^{\star}$ in the Poisson equation which has to be discretized by a usual numerical scheme like finite difference or finite element method.
3. Perform a full time step time advection in velocity space:

   $$f_h^{\star\star}(x, v) = \Pi_h f_h^{\star}(x, v - E_h^{\star}(x)\Delta t/2, v),$$

   that is to say

   $$f_h^{\star\star}(x, v) = \sum_{k=1}^{N} f_{h,k}^{\star\star}\eta_k(x, v) + \partial_x f_{h,k}^{\star\star}\psi_k(x, v) + \partial_v f_{h,k}^{\star\star}\varphi_k(x, v),$$

   where

   $$f_{h,k}^{\star\star} = f_h^{\star}(x_k, v_k - E_h^{\star}(x_k)\Delta t),$$

   $$\partial_x f_{h,k}^{\star\star} = \partial_x f_h^{\star}(x_k, v_k - E_h^{\star}(x_k)\Delta t) - \Delta t\partial_x E_h^{\star}(x_k)\partial_v f_h^{\star}(x_k, v_k - E_h^{\star}(x_k)\Delta t),$$

   $$\partial_v f_{h,k}^{\star\star} = \partial_v f_h^{\star}(x_k, v_k - E_h^{\star}(x_k)\Delta t).$$

4. Perform a second half time step advection in physical space:

   $$f_h^{n+1}(x, v) = \Pi_h f_h^{\star\star}(x - v\Delta t/2, v),$$

   that is to say

   $$f_h^{n+1}(x, v) = \sum_{k=1}^{N} f_{h,k}^{n+1}\eta_k(x, v) + \partial_x f_{h,k}^{n+1}\psi_k(x, v) + \partial_v f_{h,k}^{n+1}\varphi_k(x, v),$$

   where

   $$f_{h,k}^{n+1} = f_h^{\star\star}(x_k - v_k\Delta t/2, v_k),$$

   $$\partial_x f_{h,k}^{n+1} = \partial_x f_h^{\star\star}(x_k - v_k\Delta t/2, v_k),$$

   $$\partial_v f_{h,k}^{n+1} = -\frac{\Delta t}{2}\partial_x f_h^{\star\star}(x_k - v_k\Delta t/2, v_k) + \partial_v f_h^{\star\star}(x_k - v_k\Delta t/2, v_k).$$

3.4. Positive and conservative schemes

The previous schemes do not preserve positivity and mass. Indeed this feature comes from the interpolation operator. The nonpreservation of positivity and mass could be an inconvenience for long time simulations since numerical oscillations develop. In order to recover positivity and mass conservation we use the ideas of Priestley [29] and Gravel and Staniforth [31] which have been applied in numerical weather prediction codes.

First we are going to define the properties, we expect the solution to verify. The algorithm provides a positive solution if the solution verifies the following maximum principle:

$$f^n_{\min} \leqslant f^{n+1}_{h,l} \leqslant f^n_{\max} \quad \forall l \ \forall n, \tag{11}$$

where

$$f^n_{\min} = \min_k \{f^n_{h,k}\}, \quad f^n_{\max} = \max_k \{f^n_{h,k}\}.$$

The solution conserves the mass if

$$\sum_k f^n_{h,k} \mathscr{A}_k = \sum_k f^0_{h,k} \mathscr{A}_k = M_0, \tag{12}$$

where $\mathscr{A}_k$ is the area associated to the node N_k such that $\cup_k \mathscr{A}_k = \overline{\Omega}$.

Now we explain how to obtain a positive and conservative solution by applying it on the first half advection in the physical space. Note that the algorithm will be the same for the other advections.

Let $f^\star_{L_h}(x,v)$ be a low order solution computed according to the first step of the algorithm described previously, with the Lagrange interpolation operator of order one for example. Let $f^\star_{H_h}(x,v)$ a high order solution computed according to the first step of the algorithm described previously, with one of the Hermite interpolation operators we saw before. Let $f^\star_{L_h,k} = f^\star_{L_h}(x_k, v_k)$ and $f^\star_{H_h,k} = f^\star_{H_h}(x_k, v_k)$. We suppose that the triangle T_j contains the point $(x_k - v_k \Delta t/2, v_k)$ which is at the time t^n the departure point approximation of the characteristic curve ending at the point (x_k, v_k) at the time t^{n+1}. Let N_T the number of nodes carried by a triangle T on which we know f^n_h. We define f^+ and f^- by

$$f^+ = \max\{f^n_{h,1}, \ldots, f^n_{h,N_T}\}$$

and

$$f^- = \min\{f^n_{h,1}, \ldots, f^n_{h,N_T}\}.$$

Then we set

$$\overline{f}_k = \begin{cases} f^+ & \text{if } f^\star_{H_h,k} > f^+, \\ f^- & \text{if } f^\star_{H_h,k} < f^-, \\ f^\star_{H_h,k} & \text{otherwise.} \end{cases}$$

If $f^\star_{L_h,k} - f^\star_{H_h,k} \neq 0$ then we define

$$\gamma^{\max}_k = \frac{\overline{f}_k - f^\star_{L_h,k}}{f^\star_{H_h,k} - f^\star_{L_h,k}},$$

otherwise we set

$$\gamma^{\max}_k = 1.$$

Then, if we set

$$f^\star_{h,k} = \gamma^{\max}_k f^\star_{H_h,k} + (1 - \gamma^{\max}_k) f^\star_{L_h,k},$$

we see that the solution satisfies the maximum principle in sense of (11). In order to have a conservative solution we have to replace the set $\{\gamma^{\max}_k\}$ by the set of optimal $\{\gamma_k\}$ for which the solution still preserves the

maximum principle and the mass. In order to get a solution which preserves the maximum principle (11) the set $\{\gamma_k\}$ must satisfy the constraints

$$0 \leqslant \gamma_k \leqslant \gamma_k^{\max}.$$

Moreover, if we want that the solution preserves mass we impose the constraint (12). Let us define

$$\xi_k = (f^{\star}_{H_h,k} - f^{\star}_{L_h,k})\mathscr{A}_k$$

then the condition (12) can be rewritten as

$$\sum_k \gamma_k \xi_k = M_0 - \sum_k f^{\star}_{L_h,k}\mathscr{A}_k = M^{\star}.$$

Note that if $\gamma_k \to 1$ then we get a high order reconstruction. On the contrary we get low order reconstruction if $\gamma_k \to 0$. In order to obtain a high order reconstruction as often as possible, the problem can consist in minimizing the cost function

$$\mathscr{L}(\gamma) = -\sum_k \gamma_k,$$

where the unknowns $\{\gamma_k\}$ are subject to the constraints

$$0 \leqslant \gamma_k \leqslant \gamma_k^{\max}, \quad \sum_k \gamma_k \xi_k = M^{\star}.$$

This kind of problem can be solved by linear programming methods as the simplex method. Next we present a direct way of obtaining a solution by solving the constraints only (cf. [29]). Note that to enforce the conservation of other physical quantities such as energy, entropy or high order moments we can extend this method which leads to linear or nonlinear optimization problems with constraints. This method can also be used to minimize the loss of preserved quantities like the L^2 norm (minimization of the numerical diffusion) by defining the new cost function

$$\mathscr{L}(\gamma) = \left| \|f_h(0)\|_{L^2_h} - \|f_h(t^n)\|_{L^2_h} \right|,$$

where

$$\|f_h(t^n)\|_{L^2_h} = \left(\sum_k \left(\gamma_k (f^n_{H_h,k} - f^n_{L_h,k}) + f^n_{L_h,k} \right)^2 \mathscr{A}_k \right)^{1/2}.$$

First, if we have

$$\sum_k \gamma_k^{\max} \xi_k = M^{\star}, \tag{13}$$

the mass is conserved and we have found a positive solution which preserves the discrete maximum principle (11) and the mass conservation (12).

Now assume that

$$\sum_k \gamma_k^{\max} \xi_k > M^{\star}. \tag{14}$$

If it is not the case, without loss of generality, we put $\xi_k = -\xi_k$ and $M^{\star} = -M^{\star}$ so as to achieve inequality (14).

In order to reduce as much as possible the size of the left hand size of (14) the negative and zero terms of the sums (14) are supplied with the highest coefficient. Then this rule allows us to determine an array *iflag* such that

$$\begin{aligned} &\text{if } \xi_k \leqslant 0 \text{ then set } \gamma_k = \gamma_k^{\max}, \quad iflag(k) = 1, \\ &\text{if } \xi_k > 0 \text{ then set } \gamma_k = 0, \quad iflag(k) = 0. \end{aligned} \tag{15}$$

Now we have to compute the coefficients γ_k for which $iflag(k) = 0$. To do this we define a *surplus* as

$$surplus = M^\star - \sum_{iflag(k)=1} \gamma_k \xi_k \tag{16}$$

and an average value of γ_k as

$$\gamma_{\text{av}} = \frac{surplus}{\sum_{iflag(k)=0} \gamma_k \xi_k}. \tag{17}$$

Note that the *surplus* or all ξ_k can be negative. In that case there is no conservative solution and the best thing to do to limit as much as possible the loss of mass is to set γ_k as it was done for the initial set up (15). In other case all the values $\gamma_k^{\max}$ for which $iflag(k) = 0$ are compared with the average value γ_{av} and set equal to the average if it does not exceed all the upper bounds, that is to say

$$\text{if } \gamma_{\text{av}} < \gamma_k^{\max} \ \forall k \text{ such that } iflag(k) = 0, \quad \text{then set } \gamma_k = \gamma_{\text{av}}, \quad iflag(k) = 1.$$

On the other hand, if some coefficients $\gamma_k^{\max}$ for which $iflag(k) = 0$ are smaller than the average value γ_{av}, then those coefficients are set equal to their maximum value:

$$\text{if } \gamma_{\text{av}} > \gamma_k^{\max} \ \forall k \text{ such that } iflag(k) = 0, \quad \text{then set } \gamma_k = \gamma_k^{\max}, \quad iflag(k) = 1.$$

The other coefficients are left with $iflag(k) = 0$. Then a new evaluation of (16) and (17) is performed. The algorithm completes successfully when we find a value γ_{av} which does not exceed any $\gamma_k^{\max}$ or when $iflag(k) = 1$ for all k. Note that seeking optimal $\{\gamma_k\}$ to enforce mass conservation will sacrifice accuracy.

4. Numerical results

In this section, we present numerical results obtained in problems of plasma physics and in the propagation of charged particle beams, with different methods conservative or not. Note that conservative methods means here that the methods preserve the conservation of the global mass defined by (12) and the maximum principle defined by (11).

4.1. The one-dimensional Vlasov–Poisson system

In this section we compare different methods conservative or not, with different reconstruction techniques for the numerical resolution of the VP system with periodic boundary conditions

$$\frac{\partial f}{\partial t} + v\frac{\partial f}{\partial x} + E(t,x)\frac{\partial f}{\partial v} = 0$$

coupled with the normalized Poisson equation

$$E(t,x) = -\frac{\partial \phi}{\partial x}, \quad -\frac{\partial^2 \phi}{\partial x^2} = \int_{\mathbb{R}} f(t,x,v)\,\mathrm{d}v - 1.$$

According to the numerical scheme described in Section 3 we have to compute the gradient of the electric field. Here, this computation is easy because we see that

$$\frac{\partial E}{\partial x}(t,x) = \rho(x) - 1 = \int_{\mathbb{R}} f(t,x,v)\,\mathrm{d}v - 1.$$

4.1.1. The linear Landau damping

The initial data is

$$f(0,x,v) = \frac{1}{\sqrt{2\pi}} \exp(-v^2/2)(1 + \alpha\cos(kx)) \quad \forall (x,v) \in [0,L] \times \mathbb{R},$$

where $\alpha = 0.01$ stands for the intensity of the perturbation. The length period is $L = 4\pi$ and $v^{\max} = 6$ is the value beyond which we consider the distribution function is equal to zero. The time step is $\Delta t = 1/8$ and N_{mesh} represents the number of mesh cells. The final time $T = 50\omega_p^{-1}$.

Fig. 1 shows the comparison of the evolution of the first mode ($k = 0.5$) of the electric field, for different interpolation operators. Here the cell number (triangles) is 3906 ($\sim$32 points in x by 64 points in v) and we do neither enforce the positivity nor the mass conservation of the solution. The amplitude of the first mode $E(k = 0.5, t)$ decreases exponentially as predicted by the theory. The damping rate and the frequency of oscillations obtained by these methods are, respectively, given by $\gamma = 0.153$ and $\omega = 1.415$, which agree very well with values $\gamma = 0.1533$ and $\omega = 1.4156$ predicted by the theory. For this physical case the differences between the methods appear in long time. The best schemes are those that use $\mathscr{C}^1$ reconstructions and the less satisfactory is the Lagrange operator of order 2. On Fig. 3(a) we observe that the "recurrence effect" (see [25]) appears at $T_{\text{R}} = 33.49$, which is the theoretical time predicted from the free streaming case (i.e. without electric field) since $T_{\text{R}} = 2\pi/(k\Delta v)$. Although no conservation is enforced we observe that the distribution function remains positive and the relative error norm of variations of kinetic entropy, mass,

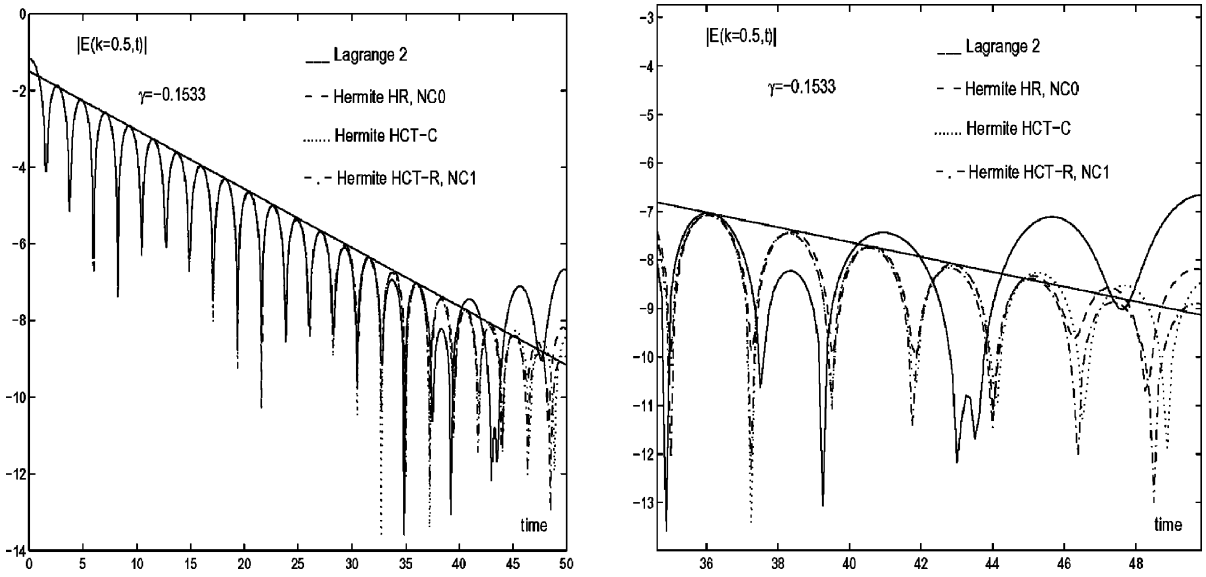

Fig. 1. Comparison of interpolation operators on the evolution of the first mode $E(k = 0.5, t)$ of the electric field for the linear Landau damping, $N_{\text{mesh}} = 3906$.

L^1-norm, L^2-norm and total energy always stay less than 10^{-5}. Figs. 2 and 3 compare for different meshes, the effectiveness of the interpolation operators and the effect of the positivity and the mass conservation enforcing on the first mode. First NC1 and HCT-C interpolation operators give very similar results. In the conservative case we observe that the evolution of the first mode in long time is less accurate but when we refine the mesh the approximation of the solution is improved. Then the algorithm seems to converge. In the conservative case (also positive) Fig. 2, the loss of accuracy arises at the same time for our scheme and the FCT or the PPM scheme (see [1]) for almost the same discretization (3960 triangles $\sim 32 \times 64$ points). The FB and CIP methods give a better accuracy for the same discretization (see [1,27]) in long time because

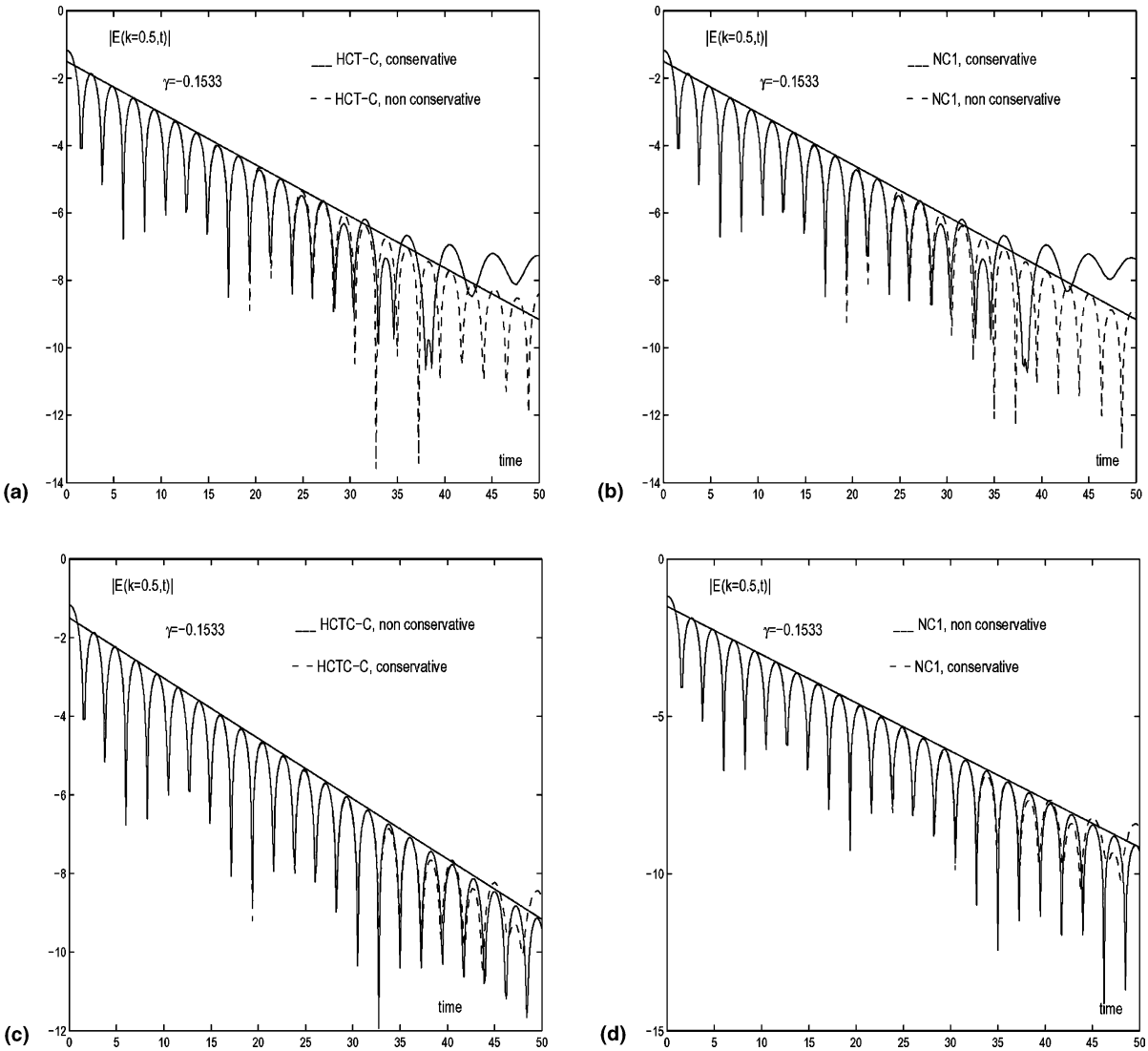

Fig. 2. Evolution of the first mode $E(k = 0.5, t)$ of the electric field for the linear Landau damping: (a,b) $N_{\text{mesh}} = 3906$; (c,d) $N_{\text{mesh}} = 7874$.

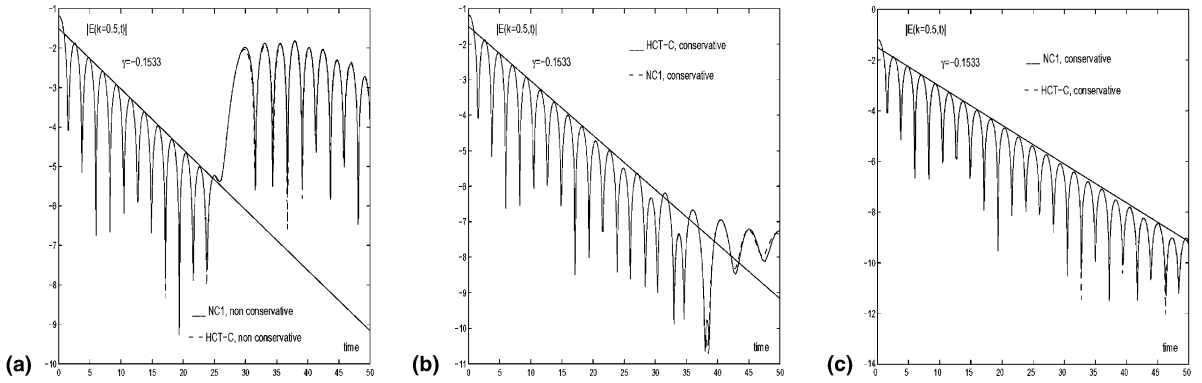

Fig. 3. Evolution of the first mode $E(k = 0.5, t)$ of the electric field for the linear Landau damping: (a) $N_{\text{mesh}} = 1092$; (b) $N_{\text{mesh}} = 3906$; (c) $N_{\text{mesh}} = 16{,}320$.

they do not preserve the positivity of the distribution function whereas the others do. Enforcing the positivity destroys the accuracy because it introduces diffusion.

4.1.2. The strong Landau damping

The initial data is

$$f(0,x,v) = \frac{1}{\sqrt{2\pi}} \exp(-v^2/2)(1 + \alpha \cos(kx)) \quad \forall (x,v) \in [0,L] \times \mathbb{R},$$

where the amplitude of the initial perturbation of the density is increased. We take $\alpha = 0.5$. We still take $L = 4\pi$, $k = 0.5$, $\Delta t = 1/8$ and $v^{\max} = 6$. The number of cells is $N_{\text{mesh}} = 2048$. The electric field introduce a strong modulation of the charge density. The previous theory cannot be applied as nonlinear effects are too important but this test has been studied by many authors [10,16,21,25,27]. The amplitude of the first mode decreases exponentially in a first time, and oscillates periodically around a constant in a second time. First the electric waves give energy to the particles, that's why we observe the exponential decrease of the first mode which contains the most of the part of electric energy. Then, after the initial condition mixing and the transitory phenomena, particles whose kinetic energy is smaller than the potential energy, are trapped by electrostatic waves around the phase velocity $v_\phi = \omega/k$, where small bumps appear preceded by small holes (Fig. 9). The trapped electrons oscillate in the wave potential with a bounce frequency which is the frequency of the envelope of the first mode (see [9,14,19,23]). When the algorithm is nonconservative we observe (Figs. 4 and 5) that with Lagrange interpolation of order two the preservation of the L^1 norm is better on short time but the scheme is too dissipative (important loss of the L^2 norm and entropy). The Hermite $\mathscr{C}^1$ type interpolation (HCT-C, HCT-R, NC1) gives good results which are similar even better in term of conservation than results obtained by cubic spline on Cartesian grid (see [16]). We observe a loss of L^1 norm less than 1.16% (6% for cubic splines on a grid for almost the same discretization, see [16]) during the transitory phenomena (strong variations of the distribution function caused by nonlinear effects) which is reduced in long time to a relative error of order 10^{-3}. We observe a loss of the L^2 norm of 10% and a growth of the entropy of 16% which stabilize in long time. On one processor of a Compaq Alphaserveur ES45 1GHz, for 100 steps and 3906 triangles in the case of the conservative method ($\sim$32 points in x by 64 points in v) the runs durations are as follows: HCT-C, 16.12s; HCT-R, 6.11s; NC1, 6.30s. Among the $\mathscr{C}^1$ interpolation techniques the best interpolation operator in term of L^1 norm conservation are HCT-R and NC1, and in term of conservation of the L^2 norm (the less diffusive) the HCT-C interpolation operator is the best. On the contrary the Lagrange interpolation of order two is twice more diffusive. The conservative

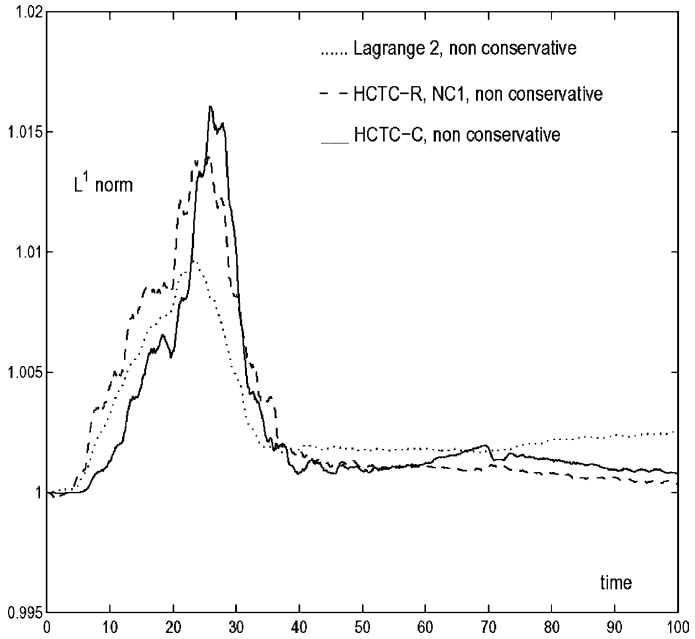

Fig. 4. Evolution of the L^1 norm for the strong nonlinear Landau damping, $N_{\text{mesh}} = 3906$.

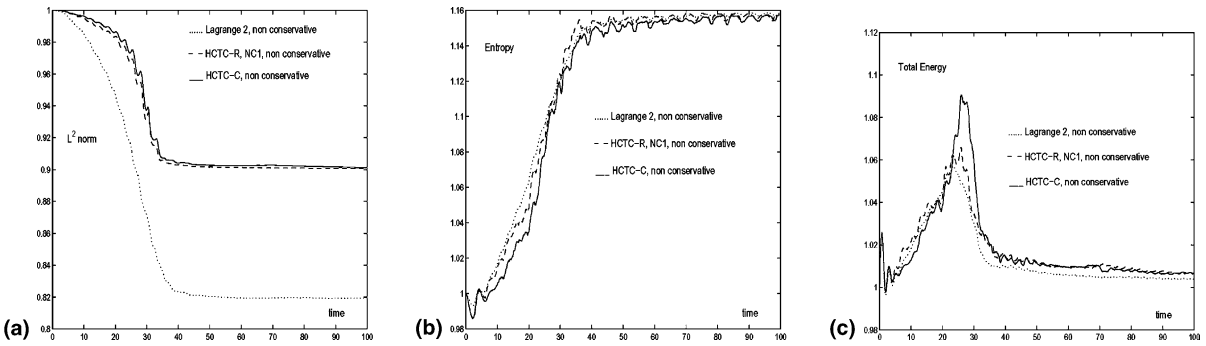

Fig. 5. Evolution of (a) L^2 norm, (b) entropy and (c) total energy for the strong nonlinear Landau damping in the case of the non-conservative algorithm, $N_{\text{mesh}} = 3906$.

version of thealgorithm does not change the results described previously except that now the solution is positive, and preserves the mass conservation (also L^1 norm) and the maximum principle (see Figs. 5–8). These conservations are useful for long simulations since numerical oscillations can develop when the nonlinear effects are dominating. Indeed if we do not search to stabilize or control the growth of these oscillations the scheme can become numerically unstable and blow up. That is what occurs with Lagrange interpolation of order 3 or more when we apply the nonconservative version of the algorithm. Moreover the decrease of the physical entropy and the L^2 norm is associated to the fact that the distribution function is smoothed when filaments become smaller than the phase space cell size. Indeed in the semi-Lagrangian method the projection onto the mesh means that we solve the Vlasov equation at the scale of the size of the

phase space cell. Then the development of thin structures is not taken into account by the scheme and the physical phenomena of high frequency are not reproduced. The projection onto the mesh plays the part of a low-pass filter.

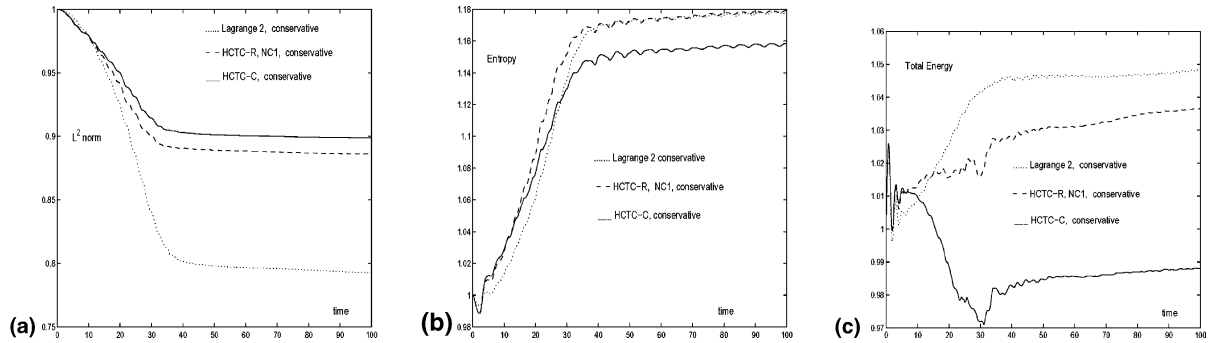

Fig. 6. Evolution of (a) L^2 norm, (b) entropy and (c) total energy for the strong nonlinear Landau damping in the case of the conservative algorithm, $N_{\text{mesh}} = 3906$.

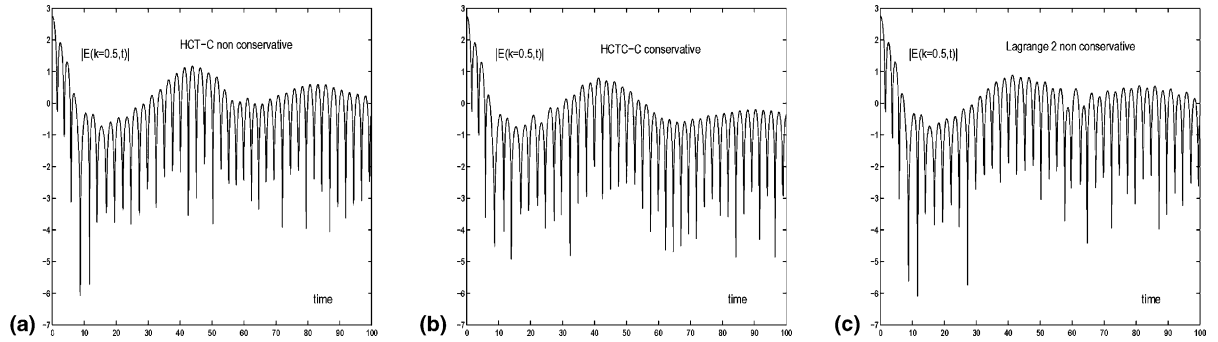

Fig. 7. Evolution of the first mode $E(k = 0.5, t)$ of the electric field for the strong nonlinear Landau damping, $N_{\text{mesh}} = 3906$. (a) HCT-C, nonconservative. (b) HCT-C, conservative. (c) Lagrange 2, nonconservative.

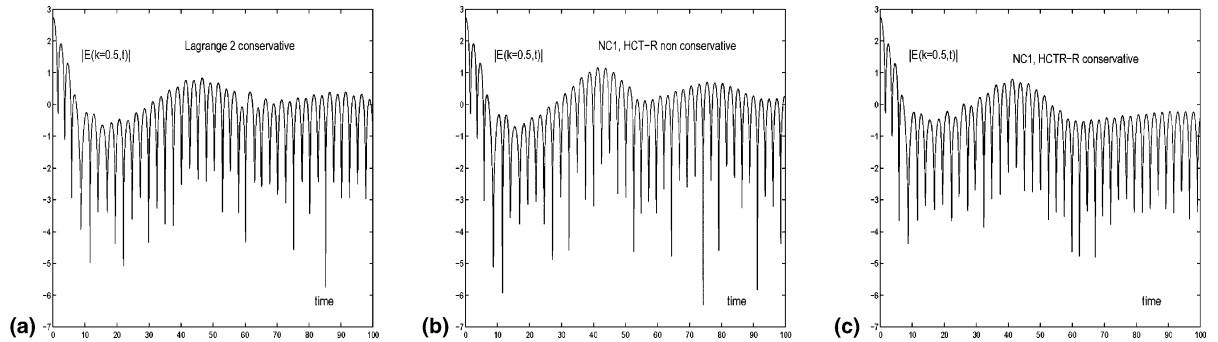

Fig. 8. Evolution of the first mode $E(k = 0.5, t)$ of the electric field for the strong nonlinear Landau damping, $N_{\text{mesh}} = 3906$. (a) Lagrange 2, conservative; (b) NC1, HCT-R, nonconservative; (c) NC1, HCT-R, conservative.

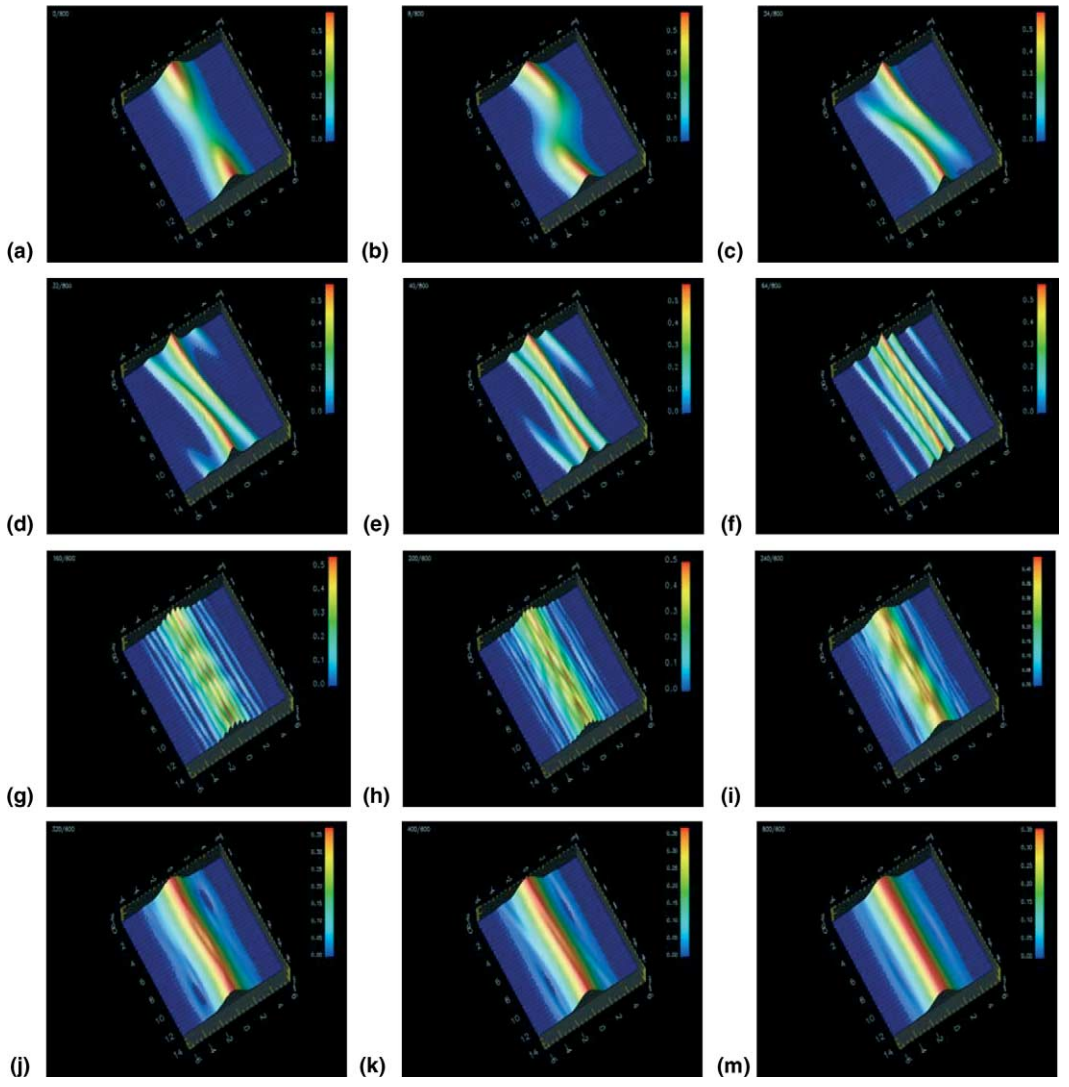

Fig. 9. Evolution of the distribution function f in phase space for the NC1 conservative scheme $N_{\text{mesh}} = 3906$, in the case of the strong nonlinear Landau damping: (a) $t = 0\omega_p^{-1}$; (b) $t = 1\omega_p^{-1}$; (c) $t = 3\omega_p^{-1}$; (d) $t = 4\omega_p^{-1}$; (e) $t = 5\omega_p^{-1}$; (f) $t = 8\omega_p^{-1}$; (g) $t = 20\omega_p^{-1}$; (h) $t = 25\omega_p^{-1}$; (i) $t = 30\omega_p^{-1}$; (j) $t = 40\omega_p^{-1}$; (k) $t = 50\omega_p^{-1}$; (m) $t = 100\omega_p^{-1}$.

4.1.3. The two stream instability

The initial condition is

$$f(0,x,v) = \frac{1}{\sqrt{2\pi}} v^2 \exp(-v^2/2)(1 + \alpha\cos(kx)) \quad \forall (x,v) \in [0,L] \times \mathbb{R},$$

where $\alpha = 0.05$, $L = 4\pi$ and $v^{\max} = 6$. The time step Δt is equal to 1/8 and $N_{\text{mesh}} = 3096$. The final time T is $100\omega_p^{-1}$.

Fig. 16 shows the time evolution of the distribution function in the phase space. At time $t \cong 10$, we observe the formation of a vortex which is associated to trapped particles. From $t \cong 10$ until $t \cong 20$, the

instability grows rapidly and a hole appears. After $t \cong 20$ the trapped particles oscillate in the electrostatic potential and the vortex rotates periodically. Figs. 13 and 14 illustrate the evolution of the first two modes $E(k = 0.5, t)$ and $E(k = 1, t)$ according to the different interpolation operators and the conservative or nonconservative version of the algorithm. After an initial transitory phase the first mode $E(k = 0.5, t)$ increases exponentially to reach its maximum at the time $t \cong 18$, then it stabilizes and oscillates slowly because of particles trapping. The other mode $E(k = 1, t)$ increases exponentially and oscillates but always stays under the first mode. The electric energy increases rapidly from $t \cong 10$ to $t \cong 20$, and then oscillates periodically (see Fig. 15).

We notice that the scheme with Lagrange interpolation of order two becomes bad in long time when we do not enforce the maximum principle and the mass conservation (see Figs. 10–12). In the case where the algorithm preserves the maximum principle and the mass conservation the Lagrange scheme of order two

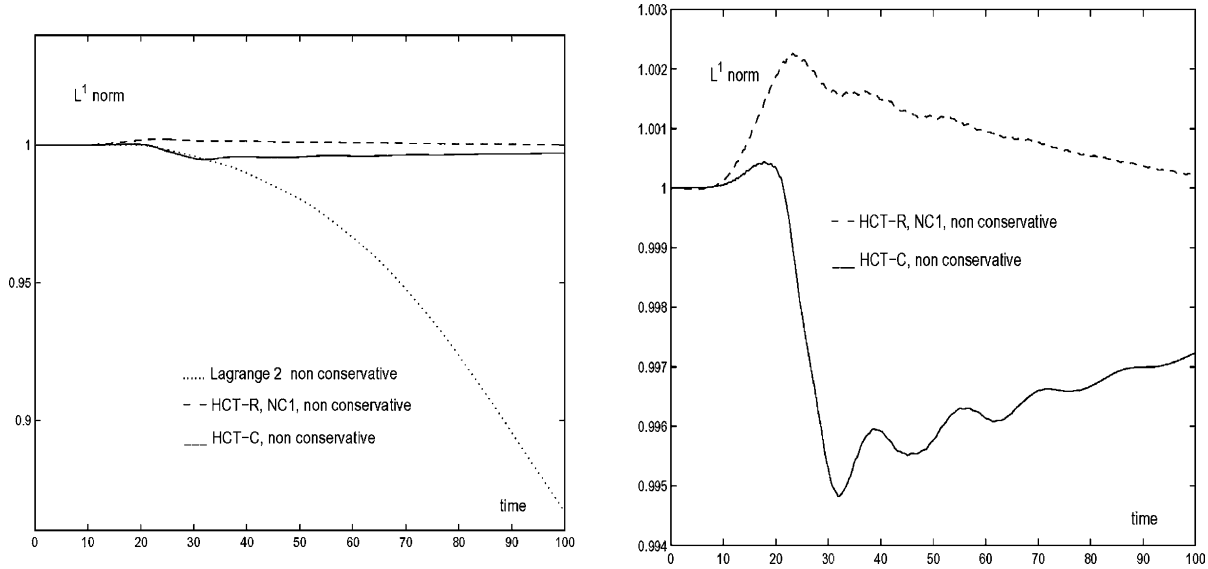

Fig. 10. Comparison of the interpolation operator on the evolution of the L^1 norm with the nonconservative scheme in the case of two stream instability, $N_{\text{mesh}} = 3906$.

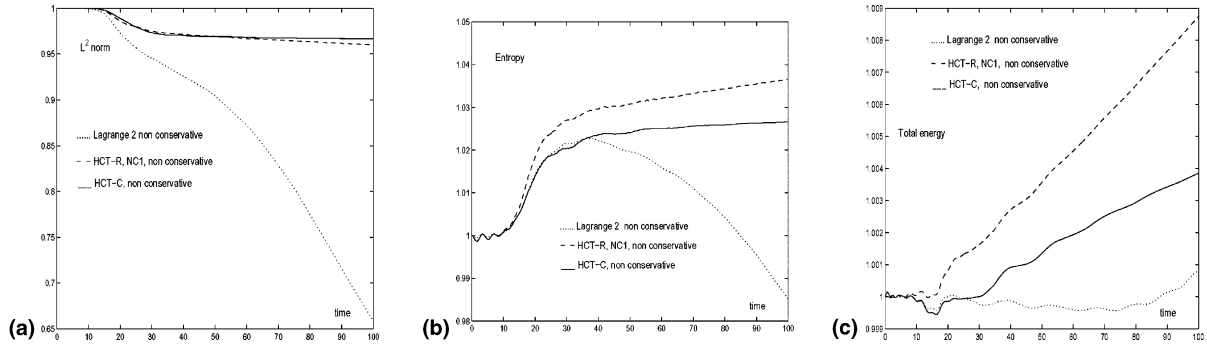

Fig. 11. Evolution of (a) L^2 norm, (b) entropy and (c) total energy, with the nonconservative scheme in the case of two stream instability, $N_{\text{mesh}} = 3906$.

gives right results even if it remains more dissipative than the other schemes (see Figs. 11 and 12). The scheme of $\mathscr{C}^1$ Hermite type (NC1, HCT-R, HCT-C) give good results. However we observe that HCT-C scheme is better in term of conservation of the entropy, L^2 norm and energy (see Figs. 11 and 12). Moreover we note that the filamentation develops from $t \cong 15$ until $t \cong 35$, and then is smoothed in long time. The

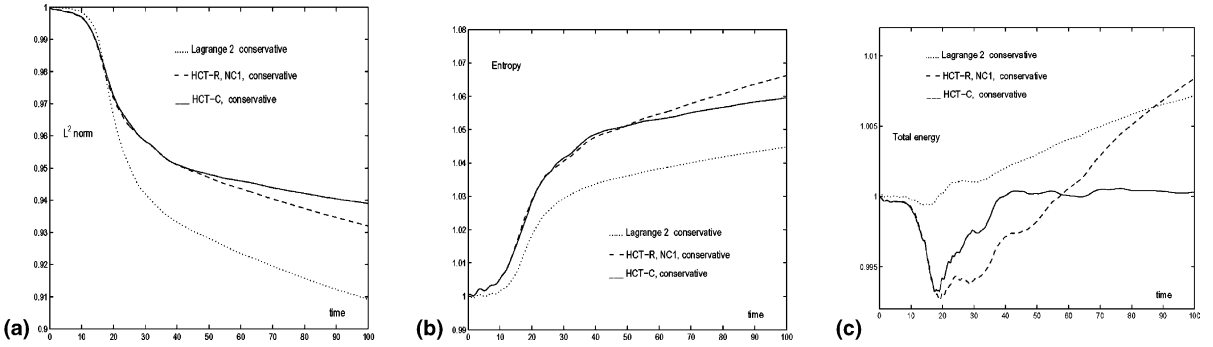

Fig. 12. Evolution of (a) L^2 norm, (b) entropy and (c) total energy, with the conservative scheme in the case of two stream instability, $N_{\text{mesh}} = 3906$.

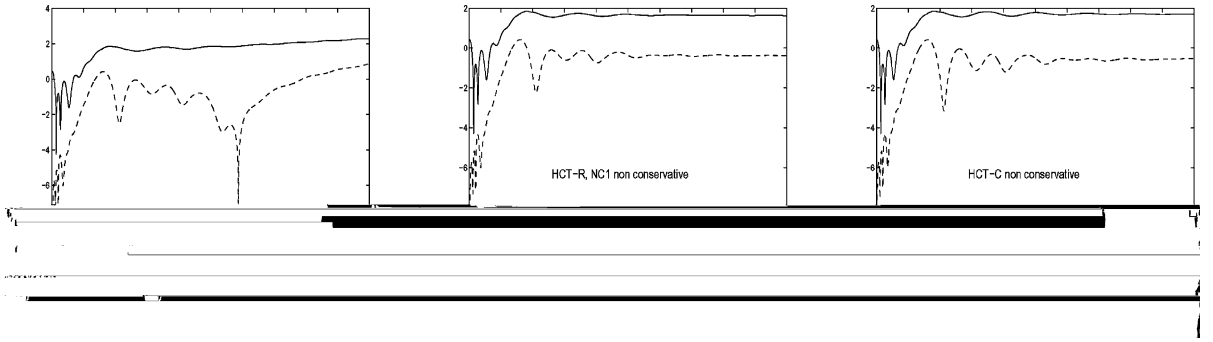

Fig. 13. Evolution of the first two modes $E(k = 0.5, t)$ and $E(k = 1, t)$ of the electric field with the nonconservative algorithm in the case of the two stream instability, $N_{\text{mesh}} = 3906$. (a) Lagrange 2, nonconservative. (b) NC1, HCT-R, nonconservative. (c) HCT-C, nonconservative.

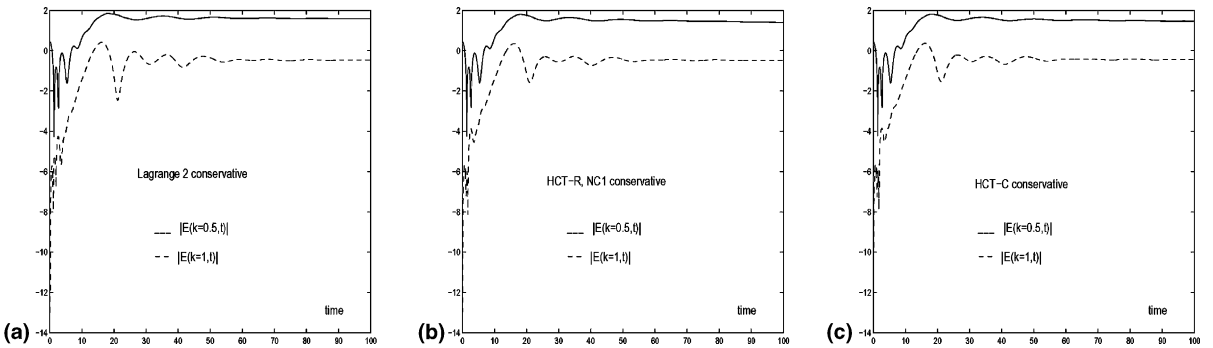

Fig. 14. Evolution of the first two modes $E(k = 0.5, t)$ and $E(k = 1, t)$ of the electric field with the conservative algorithm in the case of the two stream instability, $N_{\text{mesh}} = 3906$. (a) Lagrange 2, conservative. (b) NC1, HCT-R, nonconservative. (c) HCT-C, conservative.

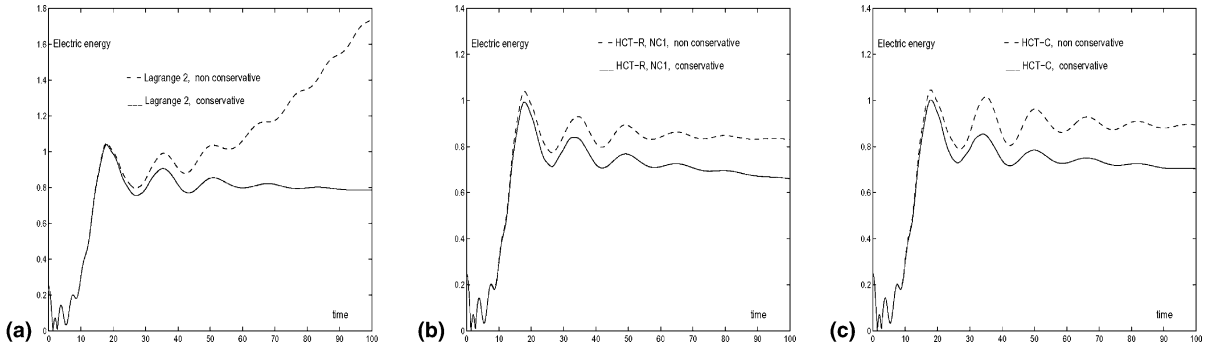

Fig. 15. Comparison of the evolution of electric energy in the case of the two stream instability, $N_{\text{mesh}} = 3906$. (a) Lagrange 2. (b) NC1, HCT-R. (c) HCT-C.

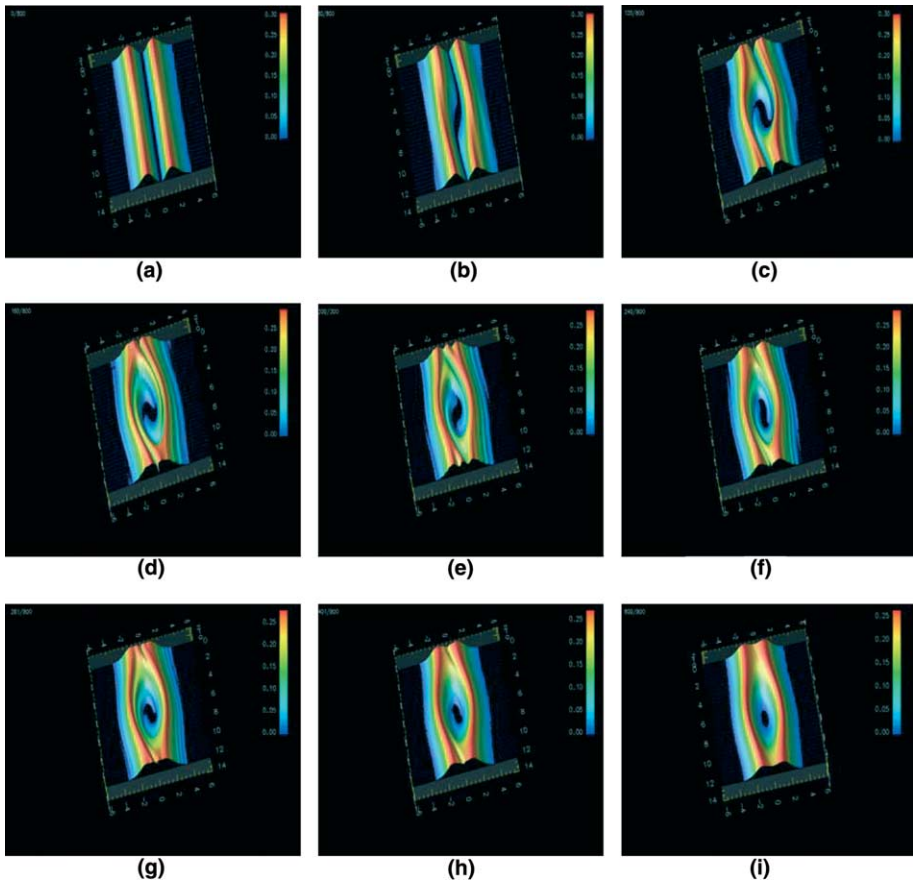

Fig. 16. Evolution of distribution function f in the phase space, with the conservative NC1 scheme and $N_{\text{mesh}} = 16{,}320$, in the case of the two stream instability: (a) $t = 0\omega_p^{-1}$; (b) $t = 10\omega_p^{-1}$; (c) $t = 15\omega_p^{-1}$; (d) $t = 20\omega_p^{-1}$; (e) $t = 25\omega_p^{-1}$; (f) $t = 30\omega_p^{-1}$; (g) $t = 35\omega_p^{-1}$; (h) $t = 50\omega_p^{-1}$; (i) $t = 100\omega_p^{-1}$.

same numerical phenomenon of filtering explained for the strong nonlinear Landau damping also occurs here.

4.2. The axisymmetric Vlasov–Poisson system

The axisymmetric VP system is very useful in the study of the propagation of charged particles beams. Here we suppose that the beam is uniform in the longitudinal variable z and propagates with constant velocity v_z. The transverse component (v_x, v_y) are small compared to the longitudinal velocity v_z. The problem is then reduced to study the classical Vlasov equation in the transverse space. Moreover we suppose that the initial data are invariant by rotation around the axis. Then the solution of the Vlasov equation still remains invariant by rotation and satisfies the following equation written in dimensionless cylindrical variables

$$\frac{\partial f}{\partial t} + v_r \frac{\partial f}{\partial r} + \left(E_s(t,r) + E_a(r,t) + \frac{v_\theta^2}{r} \right) \frac{\partial f}{\partial v_r} - \frac{v_\theta v_r}{r} \frac{\partial f}{v_\theta} = 0, \tag{18}$$

where the radial electric field $E_s(t,r)$ is given by the Poisson equation

$$\frac{1}{r} \frac{\partial (r E_s)}{\partial r} = \rho(t,r), \quad \rho(t,r) = \int_{\mathbb{R}^2} f(t,r,v_r,v_\theta)\, \mathrm{d}v_r\, \mathrm{d}v_\theta \tag{19}$$

and where the applied radial electric field $E_a(t,r)$ is supposed to be linear and equal to $-\omega_0^2 r$.

If we make the variables change $(r, v_\theta, v_r) \to (r, v_r, I)$, where $I = r v_\theta$ is the kinetic momentum in the z-direction, Eq. (18) becomes

$$\frac{\partial f}{\partial t} + v_r \frac{\partial f}{\partial r} + \left(E_s(t,r) + \frac{I^2}{r^3} - \omega_0^2 r \right) \frac{\partial f}{\partial v_r} = 0 \quad \forall I \in \mathbb{R}. \tag{20}$$

This formulation is well suited for parallelization as the variable I plays the role of a parameter.

The K–V distribution

$$f_0(r, v_r, v_\theta) = \frac{n_0}{\pi} \delta_0(2H - \beta I - a^2),$$

where n_0 is the total density, I the kinetic momentum in the z-direction, β and a two constant, and H is the transverse hamiltonian

$$H(r, v_r, v_\theta) = \frac{1}{2}(v_r^2 + v_\theta^2) + \phi_s(t,r) + \phi_a(t,r),$$

is a stationary solution of the VP equation. The K–V distribution is not the best model to represent a laboratory beam but it was studied by many authors and it is the departure point for focusing [30]. In fact, to analyze and compare the behavior of different stationary or nonstationary distributions, Lapostolle and Sacherer in 1971 introduced RMS quantities and the concept of equivalent beams. According to this concept, two beams composed of the same particles species and having the same current and kinetic energy are equivalent if the second moments of the distribution function are the same. If we consider a normalized stationary or nonstationary distribution $f(x,y,x',y')$ in four-dimensional transverse trace space where $x' = v_x/v_z$ and $y' = v_y/v_z$. The second moment in the particle coordinates x is defined by

$$\overline{x^2} = \int_{\mathbb{R}^4} x^2 f(x,y,x',y')\, \mathrm{d}x\, \mathrm{d}y\, \mathrm{d}x'\, \mathrm{d}y',$$

and the RMS beam width in the x-direction is given by

$$x_{\mathrm{rms}} = \sqrt{\overline{x^2}}.$$

In the same way we can define y_{rms}, x'_{rms} and y'_{rms}. As an example for a K–V distribution whose boundary in the $x - x'$ plane is described by a ellipse, if we consider a position where the ellipse is upright and let $x_{\max} = a$, $x'_{max} = a'$ denote the maximum x-position (radius or envelope) and maximum slope in the particle distribution, then we can show that

$$\overline{x^2} = a^2/4, \quad \overline{x'^2} = a'^2/4.$$

Then we introduce the RMS emittance ϵ_x which is a fundamental quantity in beams physics

$$\epsilon_x = \sqrt{\left(\overline{x^2}\,\overline{x'^2} - \overline{xx'}^2\right)}.$$

In order to compute the emittance ϵ_x from cylindrical coordinate, a straightforward computation shows that

$$\epsilon_x = \pi\sqrt{\overline{r^2}(\overline{v_r^2} + \overline{v_\theta^2}) - \overline{rv_r}^2},$$

where

$$\overline{r^2} = \int_{\mathbb{R}^3} r^2 f(r, v_r, I)\,\mathrm{d}r\,\mathrm{d}v_r\,\mathrm{d}I, \quad \overline{v_r^2} = \int_{\mathbb{R}^3} v_r^2 f(r, v_r, I)\,\mathrm{d}r\,\mathrm{d}v_r\,\mathrm{d}I,$$

and

$$\overline{v_\theta^2} = \int_{\mathbb{R}^3} v_\theta^2 f(r, v_r, I)\,\mathrm{d}r\,\mathrm{d}v_r\,\mathrm{d}I, \quad \overline{rv_r} = \int_{\mathbb{R}^3} rv_r f(r, v_r, I)\,\mathrm{d}r\,\mathrm{d}v_r\,\mathrm{d}I.$$

Although the emittance is constant for a K–V beam, for more general beam shapes, the emittance is not constant and increases and oscillates because of the nonlinear effects caused by the coupling between the Vlasov equation and the Poisson equation. To simulate the propagation of laboratory beams we use the model of semi-Gaussian beam, Gaussian beam and Maxwell–Boltzmann beam. The latter one is an analytical equilibrium and in order to focus the semi-Gaussian and Gaussian beams we use the the K–V distribution and the concept of equivalent beams. Indeed the initial parameters of the studied beam are computed so that its moments are the same as those of a K–V distribution.

4.2.1. The discretization of the axisymmetric Vlasov equation

For a fixed I the characteristic curves are defined by the system of ordinary differential equations

$$\begin{cases} \frac{\mathrm{d}r}{\mathrm{d}t} = v_r, \\ \frac{\mathrm{d}v_r}{\mathrm{d}t} = F(t,r) = E_s(t,r) + \frac{I^2}{r^3} - \omega_0^2 r. \end{cases} \tag{21}$$

In order to solve the axisymmetric Vlasov equation we apply our numerical method where we split the advection in physical space from the advection in velocity space. The phase space to discretize is (r, v_r, I). For the subspace (r, v_r) we use an unstructured mesh whose the boundary is a half ellipse. For the discretization of I we use a grid. However we have to choose an appropriate discretization in the I-direction. Indeed when the total electric field is linear as it is the case for a K–V distribution, the characteristic curves can be recast as

$$\frac{\omega^2}{2}r^2 + v_r^2 + \frac{I^2}{r^2} = c,$$

where c is a constant and

$$\frac{\omega^2}{2}r^2 = \left(\frac{\omega_0^2}{2} - \frac{n_0}{4}\right)r^2 = -(\phi_s + \phi_a).$$

Then, we must control the ratio I/r, and the discretization in the I-direction must verify

$$I = \pm\omega r^2.$$

Let N_I be the number of points of the discretization for the variable I. Then the mesh for I is chosen such that

$$I = \left(\frac{2a}{N_I}\right)^2 \eta\omega_0 i^2, \quad i \in \left[-\frac{N_I}{2}, \frac{N_I}{2}\right].$$

During the half time step advection in the physical space we see that we need to put an artificial boundary condition for $r = 0$. Indeed for $r = 0$ and $v_r > 0$ the particles flux is inward, whereas for $v_r < 0$ the particles flux is outward, and the particles leave the domain of computation. Then to model the crossing of particles through the axis $r = 0$ we impose a specular reflection as boundary condition for $r = 0$

$$f(0, v_r, I) = f(0, -v_r, I) \quad \forall v_r > 0.$$

During advection in velocity space step we need to compute $\partial_r F(t, r)$. Thanks to the Poisson equation (19) we obtain

$$\frac{\partial F}{\partial r}(t, r) = \rho(t, r) - \frac{E(t, r)}{r} - 3\left(\frac{I}{r^2}\right)^2 - \omega_0^2.$$

4.2.2. Semi-Gaussian beam

The initial data in Cartesian coordinate is

$$f_0(x, y, v_x, v_y) = \frac{n_0}{(2\pi v_{\text{th}}^2)(\pi a^2)} \exp\left(-\frac{1}{2v_{\text{th}}^2}(v_x^2 + v_y^2)\right)$$

if $x^2 + y^2 \leqslant a^2$ and $f_0(x, y, v_x, v_y) = 0$ if $x^2 + y^2 > a^2$. The density n_0 and the pulsation ω_0 are computed thanks to RMS quantities so that the semi-Gaussian beam is equivalent to the matched K–V beam. In fact we fix the beam radius $a = 1$, the thermal velocity $v_{\text{th}} = 1$ and the tune depression $\eta = \omega/\omega_0 = 1/4$. Then we deduce ω_0 and n_0 by the following formulae

$$v_{\text{th}} = \frac{1}{2}a\eta\omega_0, \quad \omega_0 = \sqrt{\frac{n_0}{2(1-\eta^2)}}. \tag{22}$$

We observe the formation of a space charge wave which starts at the edge of the beam and propagates inside the beam to be reflected close to the axis $r = 0$ (see Fig. 17). At the beginning the total electric field is linear inside the beam. The variations of the total electric field are small but sufficient to perturb strongly the density (see Figs. 17 and 18).

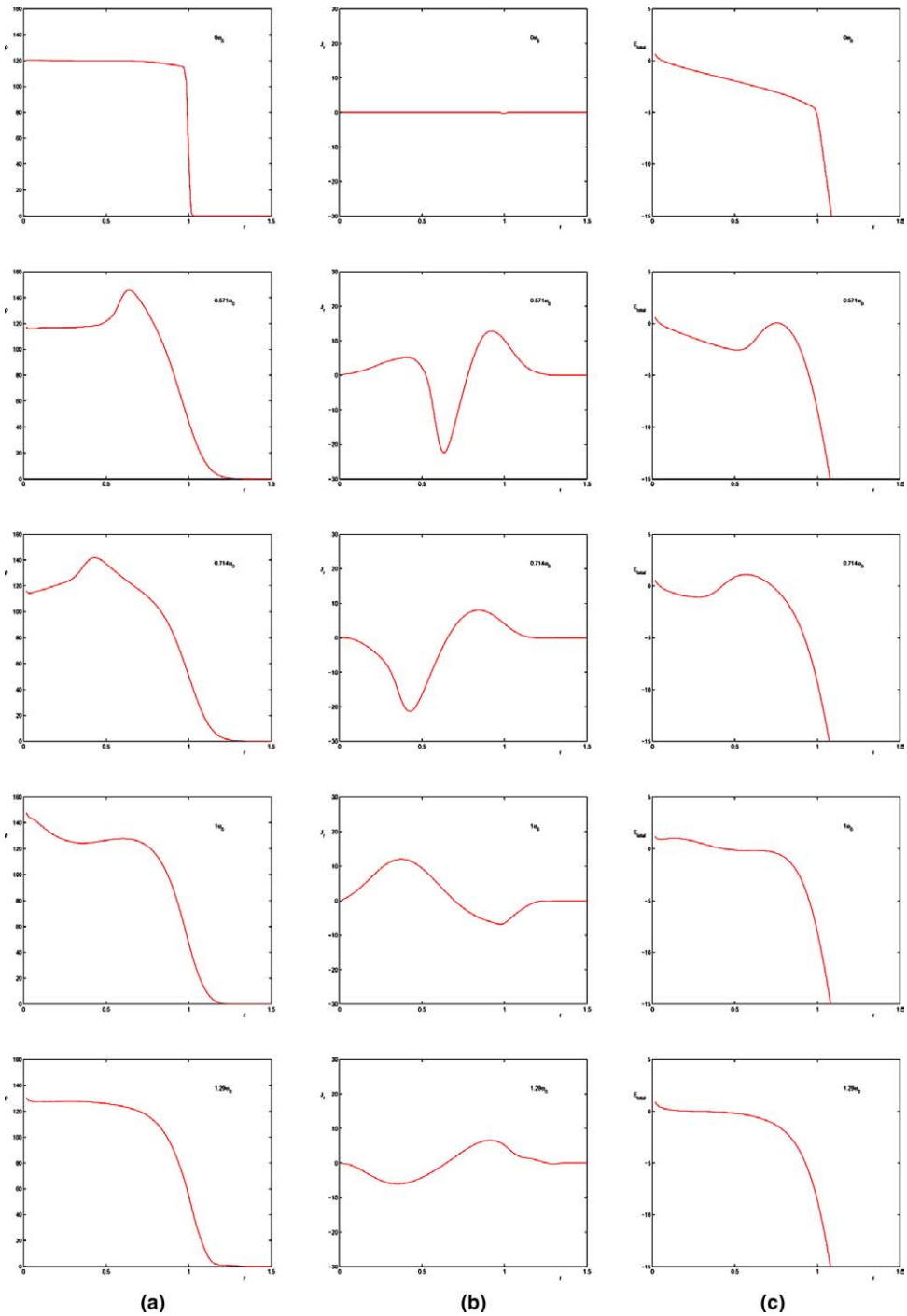

Fig. 17. Evolution of the density $\rho(t,r)$ (a), the current j_r (b), and the total force field $E_{\text{total}} = E_s(t,r) - \omega_0^2 r$ (c), with the NC1 interpolation operator at times $t = 0\omega_0^{-1}$, $0.571\omega_0^{-1}$, $0.714\omega_0^{-1}$, $1\omega_0^{-1}$, $1.29\omega_0^{-1}$, $N_{\text{mesh}} = 2{,}509{,}056$ in the case of the semi-Gaussian beam.

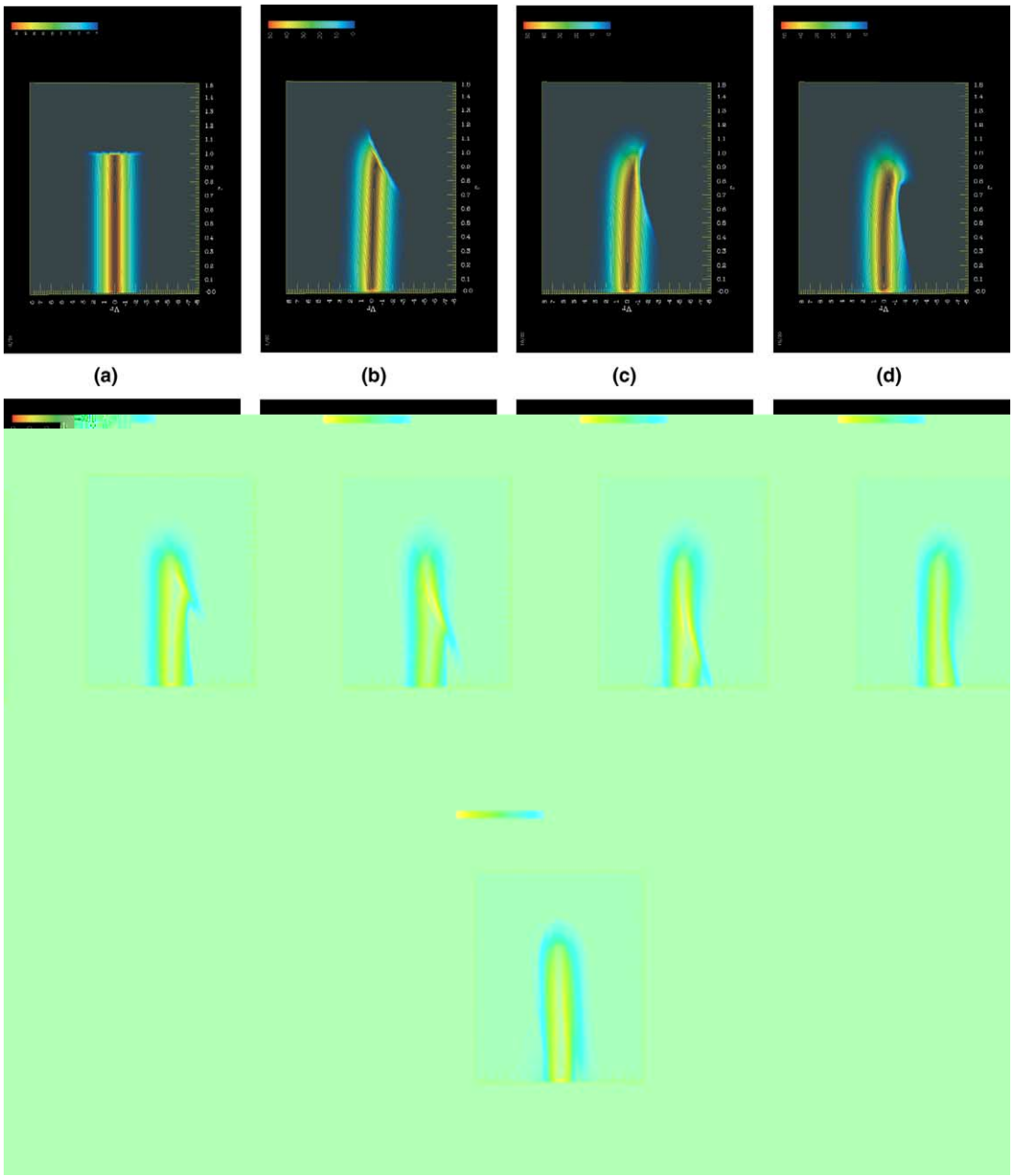

Fig. 18. Evolution of the distribution function f in the phase space (r, v_r) with the NC1 interpolation operator and $N_{\text{mesh}} = 2{,}509{,}056$, in the case of the semi-Gaussian beam. v_r is in abscissa and r in ordinate: (a) $t = 0\omega_0^{-1}$; (b) $t = 0.143\omega_0^{-1}$; (c) $t = 0.286\omega_0^{-1}$; (d) $t = 0.429\omega_0^{-1}$; (e) $t = 0.571\omega_0^{-1}$; (f) $t = 0.714\omega_0^{-1}$; (g) $t = 0.857\omega_0^{-1}$; (h) $t = 1\omega_0^{-1}$; (i) $t = 1.29\omega_0^{-1}$.

4.2.3. Maxwell–Boltzmann beam

The initial data is the normalized Maxwell–Boltzmann distribution (which is an analytical stationary solution for the VP system)

$$f_0(r, v_r, v_\theta) = \frac{\alpha}{2\pi} \exp\left(-\left(\frac{1}{2}(v_r^2 + v_\theta^2) + \phi_s(t,r) + \phi_a(t,r) \right) \right)$$

with $\phi_a(t,r) = r^2/4$, $E_a(t,r) = -\partial_r E_a(t,r)$, $0 \leqslant \alpha \leqslant 1$ and where the potential ϕ_s satisfies the Poisson equation

$$-\frac{1}{r}\frac{\partial}{\partial r}\left(r \frac{\partial \phi_s}{\partial r} \right) = \alpha \exp(-\phi_s - r^2/4)$$

solved numerically by finite differences. We take $a = 1$, $v_{th} = 1$, $\eta = 1/2$. As the Maxwell–Boltzmann distribution is a stationary analytical solution of the VP system there is no time variation of the function. Fig. 19 shows the evolution of $\log(\rho)$. Theoretically all the curves must fit the exact solution. This is the case with a precision of 3×10^{-2}. Nevertheless, for the weak densities we observe that the numerical solution differs from the exact solution because of the accumulation of diffusion error.

4.2.4. Gaussian beam

The initial data in Cartesian coordinate is

$$f_0(x, y, v_x, v_y) = \frac{n_0}{(2\pi v_{th}^2)(\pi a^2)} \exp\left(-\frac{1}{2v_{th}^2}(v_x^2 + v_y^2) \right) \exp\left(-\frac{1}{2R^2}(x^2 + y^2) \right).$$

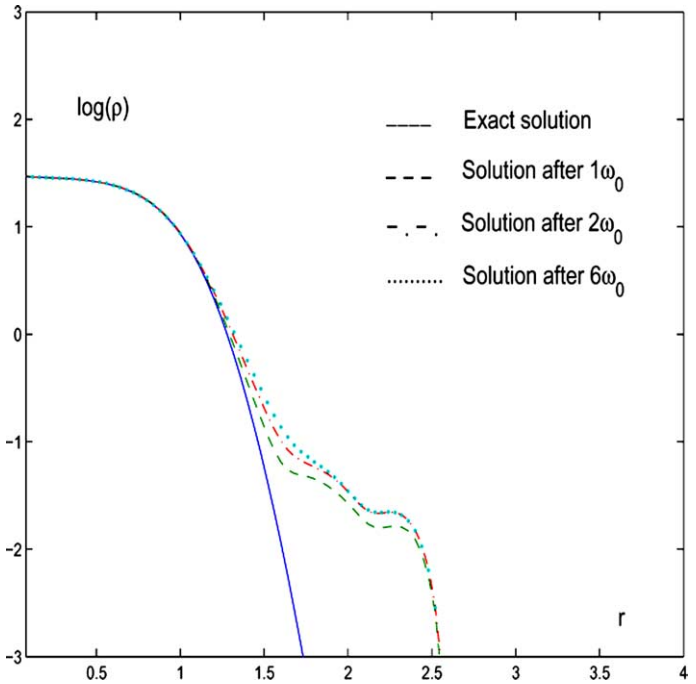

Fig. 19. Evolution of the logarithm of the density ρ with the NC1 interpolation operator and $N_{mesh} = 2{,}509{,}056$, in the case of Maxwell–Boltzmann beam.

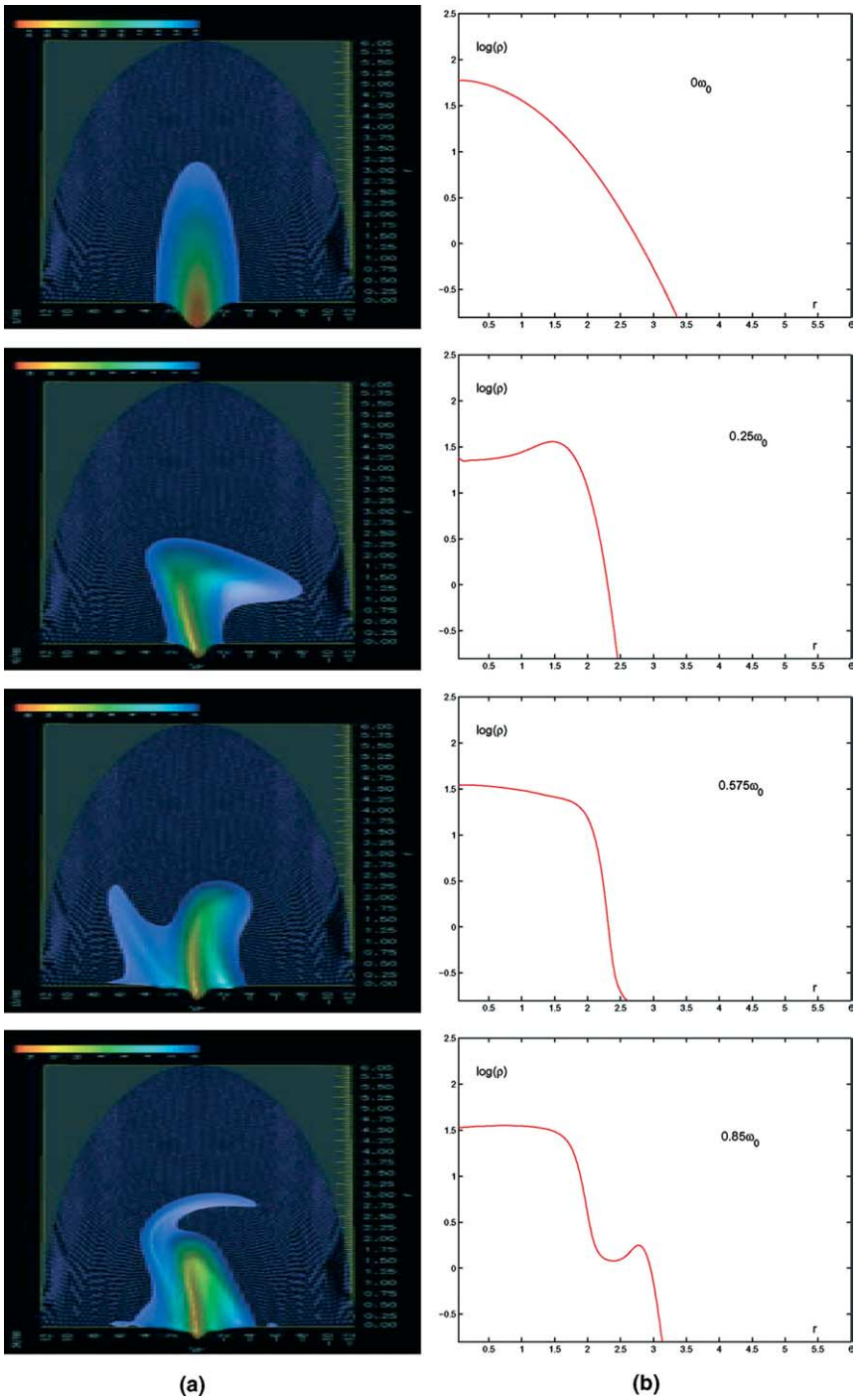

Fig. 20. Evolution of the distribution function f in the phase space (r, v_r) (a), and the logarithm of density ρ (b), with the NC1 interpolation operator at the time $t = 0\omega_0^{-1}$, $0.25\omega_0^{-1}$, $0.575\omega_0^{-1}$, $0.85\omega_0^{-1}$, $N_{\text{mesh}} = 2{,}509{,}056$, in the case of the Gaussian beam. v_r is in abscissa and r in ordinate.

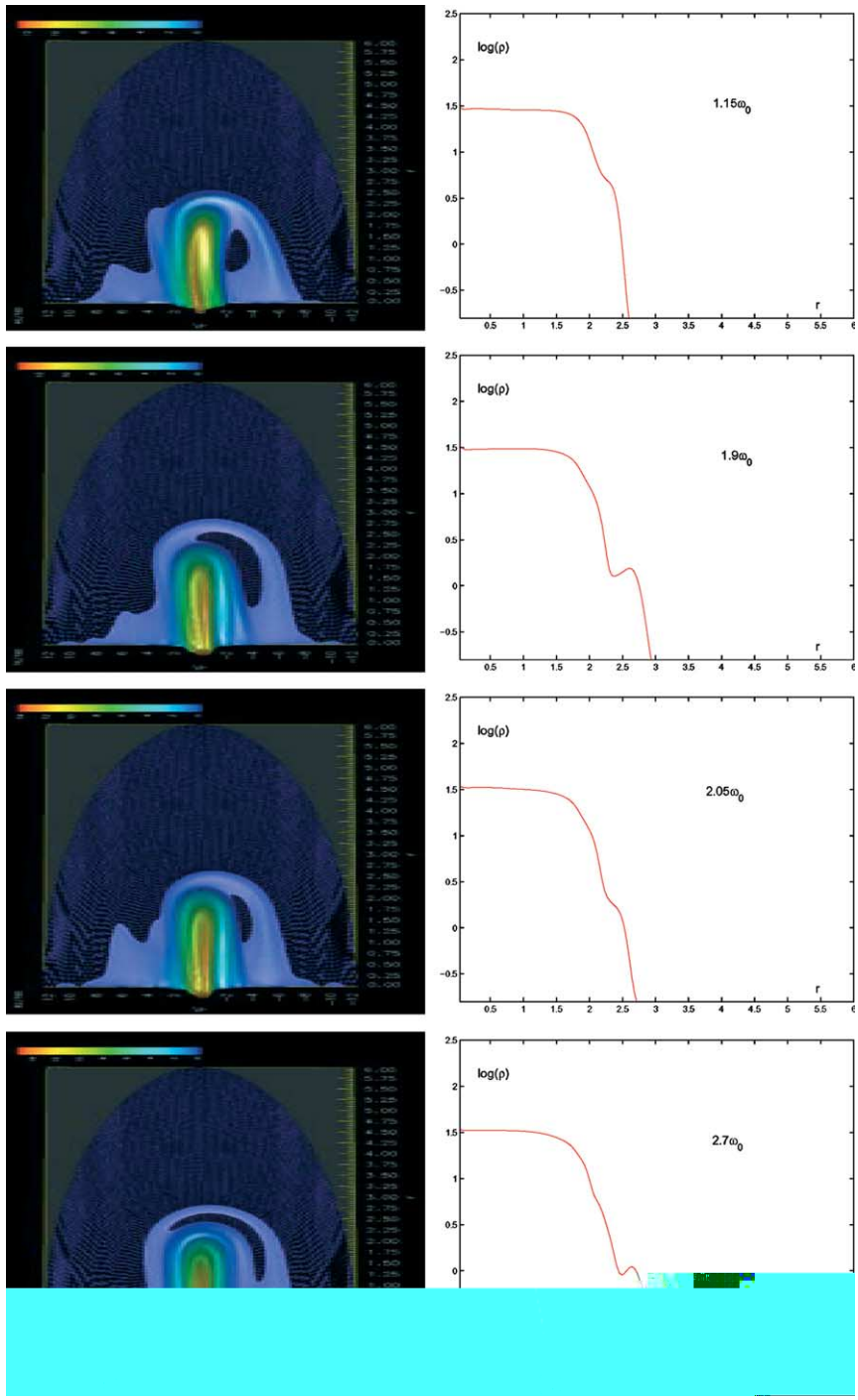

Fig. 21. Evolution of the distribution function f in the phase space (r, v_r) (a), and the logarithm of density ρ (b), with the NC1 interpolation operator at the time $t = 1.15\omega_0^{-1}$, $1.9\omega_0^{-1}$, $2.05\omega_0^{-1}$, $2.7\omega_0^{-1}$, $N_{\text{mesh}} = 2{,}509{,}056$, in the case of the Gaussian beam. v_r is in abscissa and r in ordinate.

The density n_0 the radius R and the pulsation ω_0 are computed thanks to RMS quantities so that the Gaussian beam is equivalent to the matched K–V beam. In fact we fix the beam radius $a = 1$, the thermal velocity $v_{\text{th}} = 1$ and the tune depression $\eta = \omega/\omega_0 = 1/4$. As in the Semi-Gaussian beam case we deduce ω_0 and n_0 thanks to Eq. (22). To compute R we use the following equation

$$R = a/2.$$

As in the semi-Gaussian case we observe the formation of a space charge wave which starts at the edge of the beam and propagates inside the beam to be reflected close to the axis $r = 0$ (see Figs. 20 and 21). Besides Figs. 20 and 21 show the appearance of a halo around the beam core which corresponds to the filamentation process of the distribution f in the phase space (r, v_r). The halo appears at $r = 2.6$ and halo density lies between 3% and 5% of the core beam density.

5. Conclusions

In this paper, we presented different semi-Lagrangian schemes for solving the Vlasov–Poisson system on an unstructured mesh of phase space. The time discretization is obtained by a splitting scheme which leads to the propagation of f and its gradients. Several local reconstruction techniques of high order on an unstructured mesh were considered and compared. We have checked our numerical schemes on classical benchmarks of plasma physics. Finally we have presented some applications in the propagation of charged particle beams. To go on studying beam propagation we have developed a four-dimensional parallel code (x, y, v_x, v_y) which gives satisfying results and will be the matter of a further paper.

References

[1] T.D. Arber, R.G.L. Vann, A critical comparison of Eulerian-grid-based Vlasov solvers, J. Comput. Phys. 180 (2002) 339–357.
[2] M. Bernadou, K. Hassan, Basis functions for general HCTC triangles, complete or reduced, Rapports de recherche INRIA (5) (1980).
[3] N. Besse, Convergence of a semi-Lagrangian scheme for the Vlasov–Poisson system, to appear in SIAM J. of Numer. Anal.
[4] N. Besse, Convergence of classes of high order semi-Lagrangian schemes for the Vlasov–Poisson system, in preparation.
[5] N. Besse, Convergence of a semi-Lagrangian scheme with propagation of gradients for the Vlasov–Poisson system, in preparation.
[6] C.K. Birdsall, A.B. Langdon, Plasma Physics Via Computer Simulation, McGraw-Hill, New York, 1985.
[7] J.P. Boris, D.L. Book, Solution of continuity equations by the method of flux-corrected transport, J. Comput. Phys. 20 (1976) 397–431.
[8] F. Bouchut, F. Golse, M. Pulvirenti, in: P.G. Ciarlet, P.-L. Lions, Kinetic Equations and Asymptotic Theory, Series in Applied Mathematics, Gauthier-Villars, Paris, 2000.
[9] F.F. Chen, Introduction to Plasma Physics, Plenum Press, New York, 1974.
[10] C.Z. Cheng, G. Knorr, The integration of the Vlasov equation in configuration space, J. Comput. Phys. 22 (1976) 330–351.
[11] P.G. Ciarlet, J.L. Lions (Eds.), Finite Element Methods (part 1), Vol. II, Handbook of Numerical Analysis, North-Holland, Amsterdam, 1991.
[12] P. Colella, P.R. Woodward, The picewise parabolic method (PPM) for gas-dynamical simulations, J. Comput. Phys. 54 (1984) 174.
[13] M. Crouzeix, A.L. Mignot, Analyse numérique des équations différentielles, Masson, Paris, 1992.
[14] J.L. Delcroix, A. Bers, Physique des plasmas, Tome 1 & 2 Savoirs Actuels, CNRS édition, 1994.
[15] E. Fijalkow, A numerical solution to the Vlasov equation, Comput. Phys. Commun. 116 (1999) 319–328.
[16] F. Filbet, E. Sonnendrücker, P. Bertrand, Conservative numerical schemes for the Vlasov equation, J. Comput. Phys. 172 (2001) 166–187.
[17] F. Filbet, E. Sonnendrücker, Comparison of Eulerian Vlasov solvers, Comput. Phys. Commun. 150 (2003) 247–266.
[18] R.T. Glassey, The Cauchy Problem in Kinetic Theory, SIAM, Philadelphia, PA, 1996.
[19] R.W. Hockney, J.W. Eastwood, Computer Simulation Using Particles, McGraw-Hill, New York, 1981.
[20] E. Isaacson, H.B. Keller, Analysis of Numerical Method, Wiley, New York, 1966.

[21] A.J. Klimas, W.M. Farell, A splitting algorithm for Vlasov simulation with filamentation filtration, J. Comput. Phys. 110 (1994) 150.
[22] R.J. Leveque, Numerical Methods for Conservation Laws, Lectures in Mathematics, ETH Zürich, Birkhäuser, 1992.
[23] E. Lifchitz, L. Pitayevski, Cinétique physique, Tome 10, ed. MIR 1990.
[24] G.G. Lorentz, Approximation of Functions, Holt, Rinehart & Winston, New York, 1966, 1990.
[25] G. Manfredi, Long time behaviour of nonlinear Landau damping, Phys. Rev. Lett. 79 (1997) 2815–2818.
[26] P. Mineau, Simulation en physique des plasmas, PhD Thesis, Orléans, France, 1997.
[27] T. Nakamura, T. Yabe, The cubic interpolated propagation scheme for solving the hyper-dimensional Vlasov–Poisson equation in phase space, Comput. Phys. Commun. 120 (1999) 122–154.
[28] G. Nielson, Minimum norm interpolation in triangles, SIAM J. Numer. Anal. 17 (1980) 44–62.
[29] A. Priestley, A quasi-conservative version of the semi-lagrangian advection scheme, Mon. Weather Rev. (1992) 621–629.
[30] M. Reiser, Theory and Design of Charged Particle Beams, Wiley Series in Beam Physics and Accelerator Technology, 1994.
[31] S. Gravel, A. Staniforth, A mass-conserving semi-Lagrangian scheme for the Shallow-Water equations, Mon. Weather Rev. (1994) 243–248.
[32] E. Sonnendrücker, J. Roche, P. Bertrand, A. Ghizzo, The semi-Lagrangian method for the numerical resolution of Vlasov equations, J. Comput. Phys. 149 (1996) 841–872.
[33] S.I. Zaki, L.R. Gardner, T.J.M. Boyd, A finite element code for the simulation of one-dimensional Vlasov plasmas I Theory, J. Comput. Phys. 79 (1988) 184;
II Applications, J. Comput. Phys. 79 (1988) 200.